UNIVERSITAT POLITÈCNICA DE CATALUNYA

Biomedical Engineering Doctoral Programme

OPTIMIZATION AND MUSCLE SYNERGY APPROACHES FOR STUDYING MUSCLE REDUNDANCY DURING WALKING

by Gil Serrancolí Masferrer

A thesis submitted for the degree of Doctor for the Universitat Politècnica de Catalunya

Supervised by Dr. Josep Maria Font Llagunes[1] and
Dr. Benjamin Jon Fregly[2]

[1]Department of Mechanical Engineering
(Universitat Politècnica de Catalunya)

[2]Department of Mechanical and Aerospace Engineering
(University of Florida)

Barcelona, February 2015

Agraïments

Voldria agrair sincerament a totes aquelles persones que m'han ajudat a fer possible aquesta tesi. A continuació voldria fer una especial menció d'algunes d'elles:

En Josep Maria Font, co-supervisor de la tesi des de l'inici, que sempre m'ha encoratjat en tirar endavant la tesi. A part del seu gran suport acadèmic, la seva implicació i compromís al llarg d'aquests quatre anys són d'apreciar. Sempre li agrairé que em donés l'oportunitat de fer l'estada doctoral de sis mesos a Florida.

En Benjamin Jon Fregly, co-supervisor de la tesi i cap del *Computational Biomechanics Lab* de la *University of Florida*, pel seu excel·lent rigorós treball i dedicació supervisant la tesi. Des del primer dia que vaig arribar al seu departament, m'ha guiat i ajudat, donant-me excel·lents idees i consells d'una manera amable i alhora admirable.

Els companys del *Computational Biomechanics Lab* durant l'estada: Joanathan Walter, Ilan Eskinazi, Allison Kinney, Andrew Meyer, Jennifer Jackson, Laura Li i Romain Leberre. Sempre em van ajudar i em van donar el seu suport durant l'estada a Florida, dins i fora de la universitat.

L'Ana Barjau, co-supervisora de la tesi als inicis del doctorat, pel seu suport moral i els seus consells. M'agradaria donar les gràcies tant a l'Ana com a en Joaquim Agulló per haver confiat sempre en mi i donar-me l'oportunitat de donar classes de Mecànica a l'Escola Tècnica Superior d'Enginyeria Industrial de Barcelona (ETSEIB).

En Joan Carles Monllau, cirurgià traumatòleg i cap de la Unitat de cirurgia artroscòpia de genoll a l'Institut Català de Traumatologia i Medicina de l'Esport (ICATME), que des que li vaig proposar, va acceptar col·laborar en la tesi i el seu equip va proporcionar els pacients de ruptura del lligament creuat anterior. Espero que aquesta col·laboració pugui continuar en futurs estudis.

L’Amaia Ilzarbe i en Javier Romero, que em van ajudar en fer les mesures biomecàniques pel segon estudi, i a tots els 28 subjectes voluntaris (família, amics i pacients de l’ICATME) que van col·laborar desinteressadament en l’estudi.

Els cirurgians Lluís Tresserra, Emilio González i Julio González, i els ortodoncistes Arturo i Marcos Costa, qui indirectament em varen introduir en el fascinant món de l’enginyeria biomèdica des que era petit. La seva gran capacitat de treball, precisió i excel·lent humanitat em van fascinar.

La meva mare, que m’ha donat sempre el seu suport i consells per no abandonar, i la resta de la família pel seu incondicional suport moral. I per últim, però no per això menys important, l’Esther, pel seu afecte, per les seves correccions i consells a l’hora d’escriure la tesi i per la seva paciència durant totes les nits, caps de setmana i vacances d’estiu i de Nadal que he hagut d’estar treballant en la tesi.

Acknowledgements

There have been several people who paved me the way to make this thesis a reality. I would like to take the opportunity to thank them sincerely.

Josep Maria Font Llagunes, who supervised my PhD thesis from the beginning. He always encouraged me to push this thesis forward. Apart from being grateful for his support in an academic level, I really appreciate his personal involvement through this experience. He also gave me the opportunity to do the 6-months PhD stay in Florida, which I will always be thankful for.

Benjamin Jon Fregly, head of the Computational Biomechanics Lab at the University of Florida, for his excellent rigorous work supervising my PhD thesis. From the first day he welcomed me to his lab, he has always been providing me with excellent ideas and feedback in a kindly and friendly way that truly motivated me to go on and further.

Jonathan Walter, Ilan Eskinazi, Allison Kinney, Andrew Meyer, Jennifer Jackson, Laura Li and Romain Leberre, who helped and gave me their support during my stay in Florida within and outside the Computational Biomechanics Lab.

Ana Barjau, who supervised the thesis at the beginning of the PhD, for his moral support and advice. I would like to thank Ana and Joaquim Agulló for relying on me and giving me the opportunity to teach Mechanics lessons at the Barcelona School of Industrial Engineering.

Joan Carles Monllau, head of the Knee Surgery Unit at the Catalan Institute of Trauma and Sport Medicine (ICATME), who accepted to collaborate in my thesis and redirected ACL-deficient subjects for my study. I hope that we can continue to collaborate in further studies.

Amaia Ilzarbe and Javier Romero, who helped me in the biomechanical measurements for the second study, and all 28 subjects (family, friends and patients from ICATME) who volunteered to participate in the study.

Surgeons Lluís Tresserra, Emilio González and Julio González, and orthodontists Arturo and Marcos Costa, who indirectly introduced me in the fascinating world of biomedical engineering since I was a child. Their hard work, precision and excellent humanity really captivated me.

My mother, who gave me all her support and advised me not to abandon, and the rest of my family for their unconditional moral support. And the last but not the least, Esther, for her love, her help with writing and communication skills, and her patience during all my nights, weekends, summer and Christmas holidays spent working on the thesis.

Contents

Abstract

The human body is an over-actuated multibody system, as each joint degree of freedom can be controlled by more than one muscle. Usually, optimization techniques are used to solve the muscle force sharing problem, that is, finding out how the resultant joint torque is shared among the muscles spanning that joint.

The reduction of muscle force redundancy can be achieved in several ways. Although the strategy followed by the central nervous system (CNS) to activate the muscles is not completely clear, one of the most used hypotheses to overcome this redundancy is to consider that the CNS minimizes a physiological variable. In the first study presented in this thesis, the solution to the muscle force sharing problem was approached by minimizing the sum of squared normalized muscle forces. For this purpose, a weighted cost function was designed to evaluate which muscles were more penalized in a subject with anterior cruciate ligament (ACL) deficiency during walking. The results showed that the cost function that best fitted normalized electromyography signals with muscle activations did not treat all muscles equally.

Another way to reduce muscle redundancy is using the idea that muscles are activated synergistically when performing a task. In the second study, a muscle synergy analysis was carried out to compare the muscle activation information at two levels: onset-offset activation patterns and muscle synergy components of a sample of 18 ACL-deficient subjects and a sample of 10 healthy subjects. Some differences were found at both levels, what suggests that ACL-deficient subjects alter the muscle activations of their injured leg to stabilize the joint.

Finally, in the third study, muscle synergies were used in a two-step optimization method to predict physiologically consistent muscle and knee contact forces, while calibrating muscle parameters. In the outer level, muscle parameters were calibrated; while, in the inner level, muscle activations were calculated using the current muscle parameters. The results showed that a set of muscle parameters were able to reproduce knee contact forces with high

accuracy when knee contact forces were used during the calibration process. This study shows the main differences when these forces are available for calibrating muscle parameters and when they are not. The most important differences in the muscle parameter calibration affected lateral muscles. Therefore, this fact suggests that trials where lateral muscles play a more important role should be used to obtain a better calibration when no contact forces are available.

Resum

El cos humà és un sistema multisòlid sobreactuat, ja que cada grau de llibertat pot estar controlat per més d'un múscul. Per resoldre el problema d'indeterminació en el càlcul de les forces musculars, es sol utilitzar un mètode d'optimització. Consisteix en distribuir els moments articulars resultants entre els diferents músculs que actuen a l'articulació, i per tant, estimar la força que aquests realitzen.

La reducció de la indeterminació en el càlcul de les forces musculars es pot aconseguir de diferents maneres. Malgrat que l'estratègia que fa servir el sistema nerviós central (SNC) per activar els músculs no es coneix amb exactitud, una de les hipòtesis més utilitzades per solucionar la indeterminació és el fet de considerar que el SNC minimitza una variable fisiològica. El primer estudi presentat en aquesta tesi tractava de resoldre el problema del repartiment muscular minimitzant la suma de les forces musculars normalitzades al quadrat. Per a tal fi, es va utilitzar una funció de cost ponderada per avaluar quins músculs es penalitzen més en la marxa d'un subjecte amb el lligament creuat anterior trencat. Els resultats mostren que la funció de cost que millor aproximava les activacions musculars amb el senyal d'EMG mesurat no tractava tots els músculs per igual.

Una altra manera de reduir la indeterminació en el càlcul de les forces muscular és utilitzar la idea que els músculs s'activen sinèrgicament quan l'ésser humà realitza un moviment. En el segon estudi, es presenta una anàlisi de les sinergies musculars que compara la informació de les activacions a dos nivells: en els patrons d'activació-desactivació i en els components de les sinergies musculars d'una mostra de 18 subjectes amb ruptura del lligament creuat i una mostra de 10 subjectes sans. Es van observar diferències als dos nivells, el qual suggereix que els subjectes amb ruptura al lligament creuat alteren les activacions musculars de la seva cama lesionada per tal d'estabilitzar l'articulació lesionada, en aquest cas el genoll.

Per últim, en el tercer estudi, es van utilitzar les sinergies musculars junt amb un problema d'optimització de dues etapes per tal de predir les forces musculars i de contacte al genoll de manera fisiològicament consistent, alhora que es calibren els paràmetres musculars. En el

nivell exterior de l'optimització, es calibren els paràmetres musculars, mentre que en el nivell interior, es calculen les activacions musculars amb els corresponents paràmetres musculars. Els resultats indiquen que un conjunt de paràmetres musculars pot predir les forces de contacte al genoll amb alta precisió quan es disposa de les forces experimentals de contacte al genoll durant el procés de calibratge. Aquest estudi presenta les diferències entre el cas en què s'utilitzen les forces experimentals de contacte al genoll per calibrar els paràmetres i quan no s'utilitzen. A més, suggereix que si s'utilitzessin captures biomecàniques de moviments on els músculs laterals tinguessin un rol més important que en la marxa, el calibratge dels paràmetres seria més acurat. Per tant, es podrien predir les forces de contacte al genoll amb més precisió quan no es disposa d'aquestes.

List of Tables

List of Figures

List of Symbols

α_g	weighting factors of the cost function
α_p	pennation angle
ΔM_d	allowed moment deviation from the one calculated by inverse dynamics
a	activation
a^m	activation of muscle *m*
a_t^m	activation of muscle *m* at time frame *t*
a_{res}	reserve activation
a_{syn}	muscle activations reconstructed by synergy components
a_{thres}	threshold for muscle activations
$\boldsymbol{C}(\boldsymbol{q},\dot{\boldsymbol{q}})$	vector of inertia terms of the mechanical system
d^{mj}	moment arm of muscle *m* at joint *j*
$EMG_t^{\exp}$	experimental EMG value at time frame *t*
$EMG_t^{m,norm}$	normalized EMG signal of muscle *m* at time frame *t*
EMG_t^{rec}	reconstructed EMG value at time *t*
f^{ce}	force of the contractile element of the muscle
$F_{lat\text{-}exp}$	experimental knee lateral contact force
$F_{lat\text{-}mod}$	model knee lateral contact force
$F_{med\text{-}exp}$	experimental knee medial contact force

$F_{med\text{-}mod}$	model knee medial contact force
F_{pe}^{m}	passive force
F_{0}^{m}	maximum isometric force
f	muscle force
f^{m}	muscle force of muscle *m*
$f_{\max}^{m}$	maximum isometric force of muscle *m*
F_{s}	strength of the reserve actuator
hip_{add}	hip adduction
hip_{flex}	hip flexion
hip_{rot}	hip rotation
J_{k}^{bd}	cost function terms corresponding to the biarticular muscles controlling the knee and the subsequent distal joint (ankle)
J_{k}^{bp}	cost function terms corresponding to the biarticular muscles controlling the knee and the subsequent proximal joint (hip)
J_{CMAES}	cost function minimized by CMAES $\left(J_{CMAES} = J_{CNS} + J_{cons}\right)$
J_{CNS}	weighted square sum of normalized forces
J_{cons}	cost function terms corresponding to the fulfillment of the constraints
J_{k}^{m}	cost function terms corresponding to the monoarticular muscles controlling the knee
J_{noK}	cost function terms corresponding to the monoarticular muscles controlling the knee and the ankle
$knee_{add}$	knee adduction

$knee_{flex}$	knee flexion
$knee_{sup\text{-}inf}$	knee superior-inferior
l^{ce}	length of the contractile element of the muscle
l_0^M	optimal fiber length
$\tilde{l}^M$	normalized fiber length
l^{se}	length of the series element of the muscle
l_s^T	tendon slack length
$\mathbf{M}(\boldsymbol{q})$	inertia matrix of the mechanical system
M_j	resultant moment at joint *j*
M_{jk}	resultant moment at joint *k* and time frame *j*
ma	moment arm
ma_{dev}	moment arm deviation
ma_{thres}	threshold for moment arm deviation
MeanD	mean of differences
n_{loads}	number of loads with model moment arm deviations
n_{ma}	number of muscles with non-zero model moment arm deviations
p	p-value
$\boldsymbol{q}$	vector of generalized coordinates
$\dot{\boldsymbol{q}}$	vector of the first derivative of generalized coordinates
$\ddot{\boldsymbol{q}}$	vector of the second derivative of generalized coordinates
$\boldsymbol{Q}(\boldsymbol{q},\dot{\boldsymbol{q}})$	vector of generalized forces of the mechanical system

r	correlation coefficient
sa	scale factor of muscle activations for muscles with associated experimental EMG
sl_0^M	scale factor for optimal fiber length
sl_s^T	Scale factor for tendon slack length
SV_{mod}	synergy vector of a muscle with no available EMG (design variable)
$Threshold_{on-off}$	EMG threshold to be considered activated
R^2	coefficient of determination

List of Abbreviations

ACL	anterior cruciate ligament
addmag	adductor magnus
addmagDist	adductor magnus distal
addmagIsch	adductor magnus ischial
addmagMid	adductor magnus middle
addmagProx	adductor magnus proximal
Al	left ankle
Ar	right ankle
BF	best fit
bflh	biceps femoris long head
bfsh	biceps femoris short head
CE	contractile element
CFA	cost function accuracy
CMA-ES	covariance matrix adaptation – evolutionary strategy
CNS	central nervous system
CT	computed tomography
DOF	degree of freedom
ED	extensor digitorum longus

EMG	electromyography
EW	equally weighted
GA	gastrocnemius
gaslat	gastrocnemius lateralis
gasmed	gastrocnemius medialis
GL (in Chapter 2)	gluteus
GL (in Chapter 3)	gastrocnemius lateralis
glmed1	gluteus medius anterior
glmed2	gluteus medius middle
glmed3	gluteus medius posterior
GM	gluteus maximus
GRF	ground reaction force
HA	hamstrings
HAT	head, arms and trunk
Hl	left hip
Hr	right hip
ICATME	Catalan Institute of Trauma and Sport Medicine
IL	iliopsoas
sup-inf	superior-inferior
Kl	left knee

Kr	right knee
LHS	left heel strike
LTO	left toe off
MRI	magnetic resonance imaging
MVC	maximum voluntary contraction
NC	neural command
NNMF	non-negative matrix factorization
ODE	ordinary differential equation
PE	parallel element
perlong	peroneus longus
RF	rectus femoris
RMS	root mean square
RMSD	root mean square difference
RMSE	root mean square error
RHS	right heel strike
RTO	right toe off
SE	series element
semimem	semimembranosus
semiten	semitendinosus

SENIAM	surface electromyography for the non-invasive assessment of muscles
SO / sol	soleus
SQP	sequential quadratic programming
ST	semitendinosus
SV	synergy vector
TA / tibant	tibialis anterior
tfl	tensor fascia latae
VA	vastus
VAF	variance accounted for
vasint	vastus intermedius
vaslat	vastus lateralis
VL	vastus lateralis

Chapter 1

Introduction

The current medicine is oriented to give personalized clinical evaluations reinforced with objective data. In order to achieve that goal, there is a need to develop patient-specific treatments, which involves designing computationally fast and physiologically reliable models of the human body. Computational biomechanics allows estimating physiological parameters that we cannot measure *in vivo*. In particular, the knowledge of muscle and contact forces can be useful in several medical fields, such as in surgery to predict joint mobility, in rehabilitation to follow injured subjects, or in design of assistive devices to improve the integration of orthoses or prostheses to the human body.

Since *in vivo* muscle force measurements are not possible due to their invasiveness, computational methods are used to calculate them. A typical process would start from data measured in a biomechanics laboratory. For instance, trajectories of markers attached to the body can lead to the knowledge of joint kinematics (inverse kinematics) and together with ground reaction forces (GRF) measured with force plates allow calculating resultant joint loads (inverse dynamics). However, at this point, there is indeterminacy in the muscle force calculation, since the human body has more muscles than degrees of freedom, hereinafter called as the muscle force sharing problem.

The strategy followed by the central nervous system (CNS) to activate the muscles is not fully understood. Usual methods to solve the muscle force sharing problem consist of the resolution of an optimization problem to estimate these forces, following the idea that the

CNS minimizes a physiological variable (e.g., muscle force, stress, or activation, among others) when controlling the body movement.

Electromyography (EMG) is associated to the electrical excitation of the muscles. Activation and contraction dynamics models relate muscle excitation with its exerted force. Intramuscular EMG uses a needle to measure the EMG signal directly into the muscle fibers, but it is not usual to apply it in walking or other locomotion tasks. Instead, surface EMG (electrodes placed on the skin surface) are the most used. However, they have inaccuracies due to the difficulties in measuring reliable signals, for example from deep muscles or from muscles very close to others (*crosstalk* phenomenon). In the context of biomechanics, EMG measurements can be used either for validating the muscle excitations obtained from an optimization approach, as in Chapter 2 of this thesis, or as input data to the optimization algorithm, as in Chapter 4.

Another computational method that can clarify how muscles are activated is the use of muscle synergies. This concept considers that muscles are activated synergistically, so the CNS would send a reduced number of neural commands (time-dependent activations) and each muscle would have a weighting factor at each neural command. In this case, a low-dimensional pattern (less neural commands than muscles) controls all muscle activations.

This thesis, developed within the Biomechanical Engineering Group at Universitat Politècnica de Catalunya (UPC) and the Computational Biomechanics Lab at University of Florida (UF) is motivated by the willingness to investigate the pattern used by the CNS to activate the muscles. In Chapters 2 and 3, the studies are focused on investigating whether the muscle activation pattern of an injured subject when walking is different from the pattern of a healthy subject. The hypothesis was that the muscles spanning the injured joint had altered activation patterns. The injured subjects of both studies suffered ACL-deficiency. The reason to focus the study in ACL-deficient subjects is due to the fact that 0,3‰ of the world population suffer this injury every year, especially athletes of sports requiring contact or pivoting the knee.

In particular, the goal of the first study (Chapter 2) was to investigate what cost function best fitted muscle activations with experimental EMG, using static optimization and a weighted

cost function in a single ACL-deficient subject [1]. Muscles were grouped according to their function, and several combinations of weighting factors were tested. The goal was to prove what muscles were more penalized and how the muscle activations were altered with respect to the healthy case.

The second study (Chapter 3) dealt with the investigation of muscle activation pattern differences between a sample of 18 ACL-deficient subjects and a sample of 10 healthy subjects. The differences were evaluated at two levels, on the one hand, the onset-offset time activation patterns extracted from EMG signals and, on the other hand, the muscle synergy components. This study was carried out in collaboration with the Catalan Institute of Trauma and Sport Medicine (ICATME), where all injured subjects were redirected from. All measurements were carried out in the Biomechanics Lab of UPC.

The third study (Chapter 4) was focused on predicting physiologically consistent muscle and knee contact forces while calibrating muscle parameters. Optimization methods and muscle synergies were combined to reduce the indeterminacy in the muscle force calculation in a physiological way. Since *in vivo* contact forces were known, it was a unique opportunity to validate the prediction of knee contact forces. Furthermore, fluoroscopy and a patient-specific model were available, which allowed to calculate accurate realistic model kinematics. Two approaches were presented. In the first one, knee contact forces were used during the calibration process, which was considered to lead to a physiological calibration. In the second one, which is the most usual case, no contact forces were used during calibration. The goal was to give advice on how to calibrate the model when no knee contact forces are available to obtain physiological muscle parameter values. A two-step synergy-based optimization formulation was developed. In the optimization outer level, muscle parameters were calibrated and, in the inner level, muscle activations consistent with the current muscle parameter values were calculated. Studies in Chapters 3 and 4 are about to be submitted for journal publication at the time of the thesis delivery.

Chapter 2

A weighted cost function to deal with the muscle force sharing problem in injured subjects: a single case study

2.1 Background

The force sharing problem in human gait analysis is an open subject of research. It is the consequence of over-actuation: several muscles may control the same joint degree of freedom (DOF), and thus the problem of calculating the force exerted by each muscle from the knowledge of the total wrench (force and moment) at any particular joint is essentially undetermined. Knowing the forces exerted by each single muscle is useful both for planning a rehabilitation treatment [2,3], or for designing assistive devices [4–7].

To face up to this indeterminacy, *in vivo* measurements of the muscle forces would be helpful, but they are not usual due to their invasiveness. This is where optimization processes come in: it is assumed that the central nervous system (CNS) strategy can be represented through a cost function (associated with a physiological criterion) whose minimum value yields the individual muscle forces.

Optimization techniques to solve this problem have been well-known for more than thirty years [8]. Different studies can be found in the literature focused on investigating the strategy followed by the CNS of healthy people to predict the muscle forces from the known motion using static optimization and various cost functions [9]. This approach starts with the motion capture and the calculation of the resultant joint moments, which are shared according to the chosen cost function. Many authors have proposed different cost functions

[8,10–12], which differ in the physiological variable they represent (muscle forces, muscle tensions, muscle activations…). In these cost functions all muscles are weighted equally, i.e., the weight factors associated to each muscle in the cost function have all the same value.

Muscle forces are related to muscle activations [13]. Thus, muscle forces obtained after solving the muscle force sharing problem should be consistent with experimental activation measurements. Since the normalized electromyography (EMG) signal gives information about the muscle activation, the calculated muscle activations should be compared with EMG measurements [14].

As far as the authors know, the CNS strategy of an injured subject to activate some particular muscles rather than others has not been studied extensively. The present study is devoted to the investigation of that strategy in a single injured subject, in this case suffering anterior cruciate ligament (ACL) rupture. The main function of the ACL is knee stabilization. Therefore its rupture may cause unsteadiness and cartilage damage. During rehabilitation, muscles surrounding the knee supply the function of the ruptured ACL. This suggests that this is a case where the pattern of muscle activations will be different from that of a subject with a healthy knee [15].

The contributions of this work are two-fold: the first one is the assumption that the CNS does not weight equally the muscles when trying to compensate for a lower limb injury during gait. We explored different possibilities where the muscles were weighted differently. In order to determine the cost function that best captured the specific strategy of the subject, we compared computed muscle activations with EMG measurements. The second contribution concerns the numerical implementation of the optimization problem. We solve it in two phases. Firstly, we use an evolutionary algorithm to approach the optimal forces. Secondly, those previous solutions are taken as initial guesses and the optimal forces are obtained through a deterministic algorithm. Finally, muscle activations are calculated from the muscle forces according to a Hill-type model and are compared with the normalized EMG signal.

The chapter is organized as follows: Section 2.2 describes the biomechanical model used to study the human gait and presents the optimization algorithm applied to calculate the muscle

forces; then, the experimental method and the results are presented in Section 2.3; and finally, the main conclusions of the work are drawn in Section 2.4.

2.2 Methods

2.2.1 Modeling of the human gait dynamics

A musculoskeletal model is used to represent the human body. The biomechanics simulation software OpenSim [16] was used to obtain the joint angles and the resultant joint moments from the motion capture at our biomechanics lab. The musculo-tendon units were modeled through a Hill-type formulation.

The OpenSim 3D standard model called *gait2392* [17] was scaled to the specific subject. The multi-body system consists of eight segments: two feet, two shanks, two thighs, pelvis and HAT (Head, Arms, Trunk). It has 19 DOF: the pelvis has all 6 DOF, the hips and lumbar joint are modeled as frictionless spherical joints (3x3 DOF) and the ankles and the knees are modeled as revolute joints (4x1 DOF).

The length, mass and tensor of inertia of the segments are scaled with the Scale Tool implemented in OpenSim according to the total mass and dimensions of the particular subject whose pathological gait was studied.

Following the work by Ackermann [6], eight muscles are considered for each leg which correspond to the main actuators during human gait (Figure 2.1): Iliopsoas –IL–, Gluteus –GL–, Rectus Femoris –RF–, Hamstrings –HA–, Vastus –VA–, Gastrocnemius –GA–, Tibialis Anterior –TA– and Soleus –SO–.

A model of the muscle (with a rigid tendon) is used in order to relate the muscle force with the activation of the muscle fibers in a phenomenological way. All musculo-tendon units exhibit an active behavior and a passive viscoelastic one. The active behavior is that of the muscle fibers (or contractile elements, CE), and is usually described through a Hill-type model. The passive behavior can be simply modeled through series (SE) and parallel (PE) springs and dampers, representing the tendons and the connective tissue wrapping the muscle fibers, respectively. Figure 2.2 shows that general model. Angle α_p stands for the pennation angle (orientation angle between the muscle fibers and the tendon). The pennation

angles are obtained from literature [18]. For the sake of simplicity, PE is neglected as in [6]. So, the muscle force is $f^m = f^{ce}\cos\alpha_p$. In our study, we have followed the formulation used by Ackermann [6] and Van Soest and Bobbert [19], who give two different expressions according to whether the muscle is undergoing a concentric or an eccentric contraction.

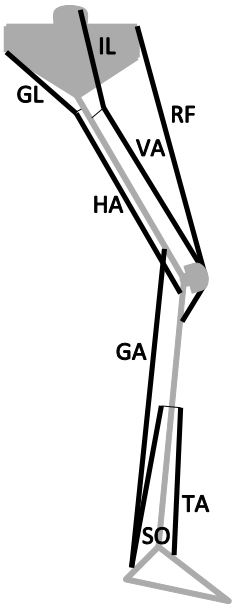

Figure 2.1. Representation of the muscles used in the model. The abbreviations coincide with those given in the text.

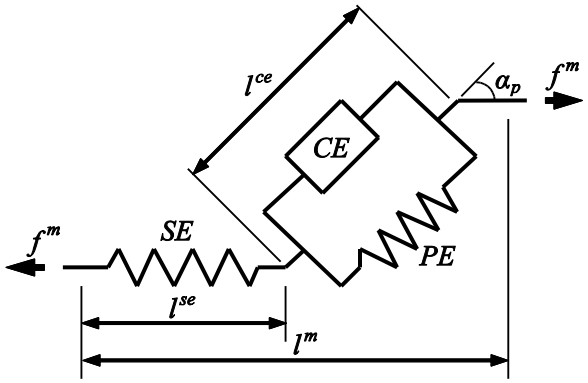

Figure 2.2. Mechanical characterization of muscle: Hill-type musculo-tendon model, adapted from [5].

2.2.2 Multi-body formulation

The application of inverse dynamics to the biomechanical multi-body system yields the resultant joint forces and moments (at the ankle, knee and hip) from the kinematics, the anthropometric parameters and the force plate measurements. The resultant flexor joint moments are associated with the muscles only, whereas the resultant forces include both

muscle and bone-to-bone forces. The biomechanics software OpenSim [16] was used to solve the inverse dynamics problem. The basic equations are:

$$\mathbf{M}(\boldsymbol{q})\ddot{\boldsymbol{q}} + \boldsymbol{C}(\boldsymbol{q},\dot{\boldsymbol{q}}) = \boldsymbol{Q}(\boldsymbol{q},\dot{\boldsymbol{q}}) \quad (2.1)$$

where $\boldsymbol{q},\dot{\boldsymbol{q}},\ddot{\boldsymbol{q}}$ are the vectors of generalized coordinates and their derivatives, $\mathbf{M}(\boldsymbol{q})$ is the inertia matrix of the system, $\boldsymbol{C}(\boldsymbol{q},\dot{\boldsymbol{q}})$ is the vector of inertia terms which depend on position and velocity, and $\boldsymbol{Q}(\boldsymbol{q},\dot{\boldsymbol{q}})$ is the vector of generalized forces. In this study $\boldsymbol{q},\dot{\boldsymbol{q}},\ddot{\boldsymbol{q}}$, $\mathbf{M}(\boldsymbol{q})$ and $\boldsymbol{C}(\boldsymbol{q},\dot{\boldsymbol{q}})$ are known, since the kinematics of the human gait is measured in the laboratory and the inertia terms are scaled.

Vector $\boldsymbol{Q}(\boldsymbol{q},\dot{\boldsymbol{q}})$ includes terms associated with joint moments and the external wrench applied to the pelvis (our unknowns), the weight of the segments (estimated from measurements) and the foot-ground contact forces and moments (measured). Note that the external wrench applied to the pelvis, also called residual wrench, should be zero if the foot-ground contact wrenches are dynamically consistent with the whole-body motion.

In order to achieve musculoskeletal dynamic consistency, the residual wrench has to be minimized. In the present study, we have run an optimization algorithm based on non-linear least squares in order to minimize these residuals while optimizing the global pelvis configuration and fulfilling equation (2.1), similar to [16].

2.2.3 Optimization for muscle force estimation

The selection of the cost function for the optimization problem is crucial. As mentioned before, the cost function represents the physiological variable minimized by the CNS during the gait. Hardt suggested that the sum of muscle forces is minimized during human gait [8]. Crowninshield and Brand proposed that fatigue, which is related to the muscle tension, is the optimized physiological variable [10]. Glitsch and Baumann applied static optimization to calculate the muscle forces for a healthy subject during walking and running comparing the minimization of the two variables [20]. They concluded that the best correspondence with the EMG was obtained when the muscle stresses were minimized.

Cost functions for the case of pathological gait have not yet been deeply studied. One reason could be a higher variability: in contrast with those associated to healthy people, gait cost

functions in case of injury may vary from one subject to another depending on the specific pathology and subject ability. Our hypothesis is that the CNS of subjects suffering from a joint pathology weights every muscle in a different way and thus cost functions weighting equally all muscles are no longer valid. The particular distribution of muscle weighting factors depends on the particular joint injury.

Accordingly, the choice of the cost function was based on the idea that the muscles controlling the injured joint had to be treated differently from the others. Grouping the muscles so that no muscle was counted twice, we came up with four different muscle sets:

- Monoarticular muscles controlling the injured joint (monoarticular muscles).

- Biarticular muscles controlling the injured joint and the subsequent proximal joint (biarticular-proximal muscles).

- Biarticular muscles controlling the injured joint and the subsequent distal joint (biarticular-distal muscles).

- Muscles not controlling the injured joint (other muscles).

Note that for some particular cases the biarticular muscles may not be split into two groups. For our particular application case the injured joint is the knee and the corresponding cost function is the following:

$$J_{CNS} = \alpha_1 J_K^m + \alpha_2 J_K^{bp} + \alpha_3 J_K^{bd} + \alpha_4 J_{noK} \tag{2.2}$$

where $\alpha_g \left(g = 1,\ldots,4\right)$ are the weighting factors associated to each group, J_K^m is the cost function term corresponding to the monoarticular muscles controlling the knee, J_K^{bp} that of the biarticular muscles controlling the knee and the subsequent proximal joint (hip), J_K^{bd} that associated with the muscles controlling the knee and the subsequent distal joint (ankle), and J_{noK} that taking into account all the other muscles:

$$J_K^m = \left(\frac{f^{VA}}{f_{\max}^{VA}} \right)^2 \tag{2.3}$$

$$J_K^{bp} = \left(\frac{f^{HA}}{f_{\max}^{HA}} \right)^2 + \left(\frac{f^{RF}}{f_{\max}^{RF}} \right)^2 \quad (2.4)$$

$$J_K^{bd} = \left(\frac{f^{GA}}{f_{\max}^{GA}} \right)^2 \quad (2.5)$$

$$J_{noK} = \left(\frac{f^{IL}}{f_{\max}^{IL}} \right)^2 + \left(\frac{f^{GL}}{f_{\max}^{GL}} \right)^2 + \left(\frac{f^{TA}}{f_{\max}^{TA}} \right)^2 + \left(\frac{f^{SO}}{f_{\max}^{SO}} \right)^2 \quad (2.6)$$

In those expressions, f^m and $f_{\max}^m$ stand for the force and maximum isometric force associated with muscle $m\,(m=1,\ldots,8)$. All α_g combinations were calculated, from $\alpha_g = 0.1$ to $\alpha_g = 0.7$, with intervals of 0.1 and satisfying that $\sum_{g=1}^{4} \alpha_g = 1$.

The optimization problem consists of minimizing the cost function at each time frame while guaranteeing the following constraints and boundary conditions:

• Equality between the moments exerted by the muscles and the resultant joint moments obtained by means of the inverse dynamics:

$$M_j = \sum_{m=1}^{8} f^m d^{mj}, \quad j = 1,2,3. \quad (2.7)$$

where M_j is the moment at joint j (1-hip, 2-knee, 3-ankle) calculated by inverse dynamics and d^{mj} is the moment arm of the muscle m at the joint j.

• Muscle force and activation boundary conditions:

$$0 < f^m < f_{\max}^m \quad (2.8)$$

$$0 < a^m < 1 \quad (2.9)$$

where a^m is the activation of muscle $m\,(m=1,\ldots,8)$. The Hill's model described in Section 2.2.1 was used to calculate a^m from f^m.

Each optimization problem was solved in two steps (Figure 2.3). First, following the strategy used in other biomechanical studies [21,22], the evolutionary algorithm called "Covariance Matrix Adaptation Evolution Strategy" (CMA-ES) was used [23], in order that the design

variables (muscle forces) approach the optimal solution. Being an evolutionary algorithm, this optimum solution is more likely to correspond to a global minimum than to a local minimum. Since the code does not allow constraints, equation (2.7) was introduced in the cost function:

$$J_{CMAES} = J_{CNS} + J_{cons} \tag{2.10}$$

where J_{CNS} represents the weighted square sum of the normalized forces defined in equation (2.2) and J_{cons} represents the fulfillment of the constraints, that is:

$$J_{cons} = \sum_{j=1}^{3} \left[\left(M_j - \sum_{m=1}^{8} f^m d^{mj} \right) \Big/ \Delta M_d \right]^2 \tag{2.11}$$

where ΔM_d is the allowed deviation from the moment calculated by inverse dynamics. When the sum of the simulated muscle moments becomes higher or lower than these bounds, the cost function term increases, since the term is squared. The boundary conditions for this step are equations (2.8) and (2.9).

In the second step, a deterministic algorithm was used. That algorithm uses a sequential quadratic programming (SQP) method to find the minimum of constrained nonlinear multivariable functions. It is implemented in a default optimization library of the Matlab software called *fmincon*. The problem was slightly different than the previous one, since the constraints were not introduced in the cost function as they were taken into account by the algorithm itself. The cost function has the form of equation (2.2), constraints of equation (2.7) and the boundary conditions of equations (2.8) and (2.9).

The reason for using these two algorithms is that although the evolutionary algorithm has a higher computational cost than the deterministic one and does not reach the solution, it is more likely to stop near the global minimum. Alternatively, the deterministic algorithm would be more likely to reach a local minimum for any choice of initial conditions. But with the results of the CMA-ES algorithm as initial guesses, the algorithm is more likely to reach the global minimum.

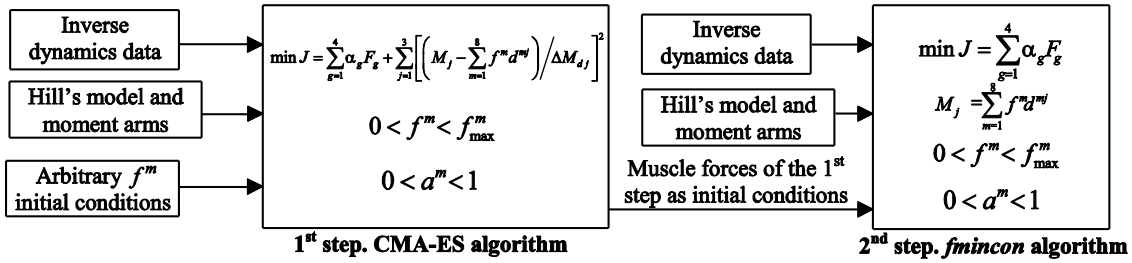

Figure 2.3. Block diagram of the two-step optimization strategy.

2.3 Results and discussion

The results are presented in this section. First, we describe the experimental method that was used to measure the kinematics and the foot-ground contact forces. Then, we introduce a brief review of the kinematic and dynamic results. The third and main subsection contains the optimization results, used to select the cost function that best fits the EMG measurements (which will be called BF cost function, where BF stands for "best fit"). In the fourth subsection, the muscle forces and activations are shown for two strategies, the one considered as the most suitable (BF) and the one using an equally weighted (EW) cost function, which is considered to be followed by a healthy subject. Finally, the values of the cost function terms are analyzed for the mentioned strategies.

2.3.1 Experimental methods

The gait of a 59-year-old male subject (weight: 90 kg, height: 1.85 m), suffering an ACL rupture at the right knee, was captured in our biomechanics lab. The subject was asked to walk as naturally as possible without any external aid. The trajectories of 22 markers attached on the skin of the subject were captured. These trajectories were captured at 100 Hz by means of 14 infrared cameras (NaturalPoint, Corvallis, OR), and they were filtered with a third order Butterworth low-pass filter with a cut-off frequency of 6 Hz.

Since the skin is a soft tissue and there is a relative movement between it and the bones, kinematic consistency was ensured running the Inverse Kinematics Tool implemented in OpenSim [16] and joint angles were obtained. Then, running the Inverse Dynamics Tool, resultant joint moments were calculated. Dynamic consistency was ensured optimizing the positions of the pelvis as explained in Section 2.2.2.

The foot-ground contact forces were measured with two force plates (AMTI, Watertown, MA) with a sample frequency of 100 Hz. These data were also filtered with a third order Butterworth filter with a cut-off frequency of 6 Hz. The walking cycle was defined as the interval between two consecutive heel-strikes for the right leg, and between two toe-offs for the left leg.

EMG measurements were also done with an 8-channel surface EMG sensor (Biometrics, Newport, United Kingdom) at 1000 Hz. One sensor was placed on each muscle, following the Surface Electromyography for the Non-Invasive Assessment of Muscles (SENIAM) recommendations [24]. The EMG signal represents the myoelectric signals produced by the physiological variations at the both sides of the muscle fiber membranes when the muscle contracts and relaxes. A higher signal indicates higher muscle activation. The signal has to be filtered, smoothed and normalized to obtain an activation signal [25]. EMG data were filtered using an RMS filter (window length: 30 frames, overlap: 10 frames), then they were filtered again with a third order Butterworth filter at 6 Hz. Finally, they were normalized to the maximum voluntary contraction (MVC) value that was recorded previously. Thus, the resultant EMG signal was kept between 0 to 1. Markers data, foot-ground contact forces and EMG data were synchronized using an own Matlab code. Scaling process, Inverse Kinematics and Dynamics analyses were performed in OpenSim.

2.3.2 Kinematic and dynamic data

The injured subject had no difficulties in walking some strides in the lab with a self-selected speed of 1.06 m/s, although he mentioned knee pain when doing certain movements. The kinematic measurements showed that the flexion-extension range of motion of the non-injured knee (62.49º) was higher than the injured knee (53.73º) (Figure 2.4). This is in agreement with the fact that the flexion of the injured knee is lower to prevent a destabilization of the knee, as it reported by Rudolph et al. [26] and Chmielewski et al. [27].

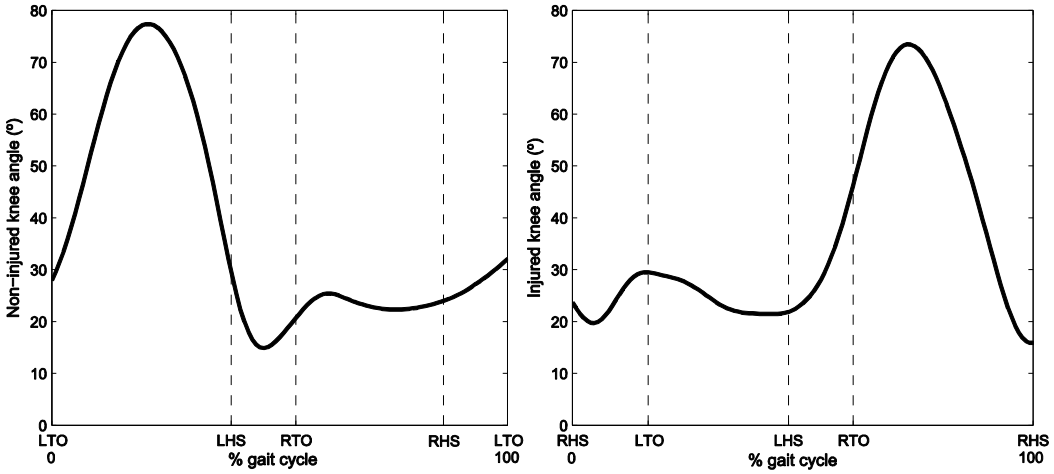

Figure 2.4. Knee flexion angles for the non-injured knee (left) and the injured knee (right). LTO stands for Left Toe Off, LHS Left Heel Strike, RTO Right Toe Off and RHS Right Heel Strike.

Figure 2.5 shows the comparison between the joint moments (obtained through inverse dynamics results) and the data found in literature for healthy people [28]. All the plots are mostly between the two standard deviations of the joint moments of healthy subjects. Focusing on the knee, the comparison between the left (non-injured) and the right (injured) moment shows a difference in the maximum values. The extension knee moment shows two peaks that correspond to the effort of that joint to maintain the leg stretched at the beginning and the end of the stance phase (highlighted in the figure with arrows). For the injured leg, these two peaks take values of 0.398 Nm/kg and 0.227 Nm/kg respectively, while for the non-injured leg they are 0.425 Nm/kg and 0.359 Nm/kg. The absolute value of ankle plantar flexion moment peak (negative in the figure and also highlighted) is higher at the injured limb (1.441 Nm/kg) than at the non-injured limb (1.143 Nm/kg). This means that the ankle contribution for the injured leg to the total support is higher, whereas the knee contribution is lower, which is in agreement with [29].

This fact has been observed by other authors. For example, according to Berchuck et al. [30], the reduction of the knee moment at the injured leg is caused by the fact that the patient modifies the forces of the knee muscles to avoid pain. In particular, the use of the quadriceps is avoided (quadriceps-avoidance gait) to minimize the anterior displacement of the proximal end of the tibia. More recently, some authors that have worked at the level of EMG signals mention that it is not just a reduction of the quadriceps force that produces the difference in the knee extension, but an activation of antagonist muscles [31,32].

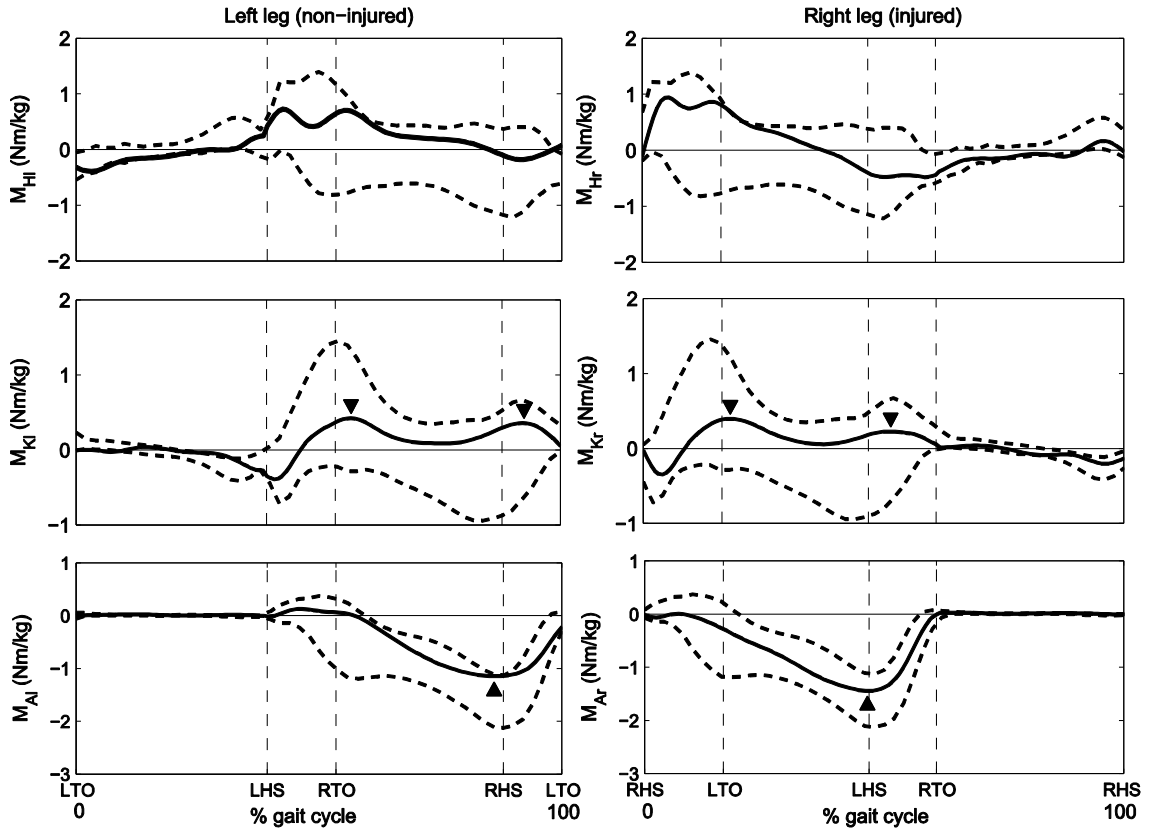

Figure 2.5. Resultant joint moments at the left leg (healthy leg) –left-, and at the right leg (injured leg) –right-. Hip and knee moments are positive in extension and ankle moment is positive in dorsiflexion. The solid curves correspond to the calculated resultant moments, and the dashed curves, to the range of two standard deviations for healthy people [28]**. The gait cycle of the left leg starts at the left-toe-off, and the right leg cycle starts at the right-heel-strike. Vertical dashed lines correspond to the events of the cycle (LTO, LHS, RTO, RHS).**

2.3.3 Optimization results

As mentioned in Section 2.2.3, up to 85 combinations of the weighting factors were tested, each of them leading to a two-step optimization problem that was solved in Matlab (Mathworks, Natick, MA) using the parallel computing toolbox. In order to quantify the accuracy of the results, i.e., to see how close the muscle activations were to the normalized EMG, we defined the cost function accuracy (*CFA*) as

$$CFA = \sum_{t=0}^{t_f} \sum_{m=1}^{8} \left(a_t^m - EMG_t^{m,norm} \right)^2 \tag{2.12}$$

where a_t^m is the activation of muscle m $(m = 1,\ldots,8)$ at time t calculated using the equations derived from a Hill-type model [6,19]. $EMG_t^{m,norm}$ is the normalized EMG signal of muscle m at time t. We assume that lower *CFA* values correspond to cost functions more consistent with the real actuation strategy.

As aforementioned, the cost function represents the variable minimized by the CNS when walking. Therefore, the comparison of the sum of the cost function values during the whole gait cycle $\sum_{t=0}^{t_f} J_{CNS}$ among all optimizations should be an indicator of the correctness of that function. We proceeded to calculate those values and compared them to the *CFA* values for the 85 combinations of the weights α_g. The result is shown in Figure 2.6. The labels indicate the weighting factors combinations, see Table 2.1.

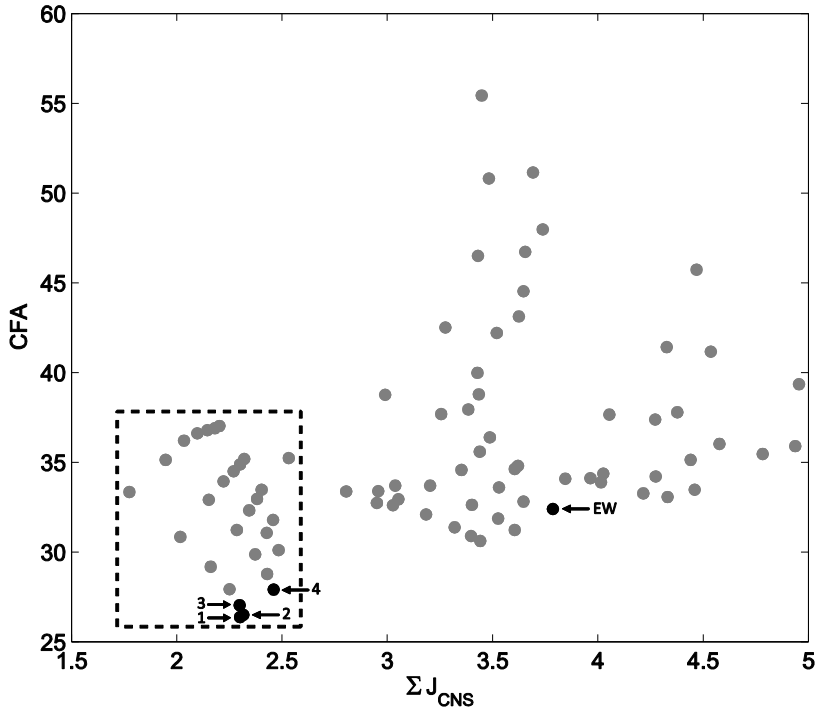

Figure 2.6. *CFA* values versus J_{CNS} for the 85 combinations of weighting factors.

The results within the dotted rectangle in Figure 2.6 correspond to reasonable low values of J_{CNS}. Among them, only those having a low *CFA* value can be considered acceptable guesses. The best four results are numbered.

Table 2.1. Results using the 4 combinations with the lowest *CFA* values and the equally weighted (EW) cost function (associated with healthy gait).

	α_1	α_2	α_3	α_4	CFA	$\sum_t J_{CNS}$
1 (Best fit, BF)	0.1	0.7	0.1	0.1	26.39	2.302
2	0.2	0.6	0.1	0.1	26.51	2.315
3	0.3	0.5	0.1	0.1	27.05	2.299
4	0.1	0.6	0.2	0.1	27.90	2.460
Equally weighted, EW	0.25	0.25	0.25	0.25	32.41	3.785

The result corresponding to the CNS of a standard healthy subject (EW) has both higher sum of *CFA* and J_{CNS} values compared to the 4 numbered cases. Therefore, the strategy followed by the studied subject to activate the muscles would be closer to penalize RF and HA (higher α_2) than weighting all muscles equally. These results support the hypothesis of this study that the CNS doesn't weight all muscles equally when activating them. Similar conclusions were reached in other studies found in the literature that support the idea that neuromuscular control plays an important role in joint stability, especially in ACL-deficient knee [15].

2.3.4 Muscle forces and activations

The muscle forces and activations of the injured leg obtained in the two-step static optimization for the BF and EW cost functions are shown in Figures 2.7 and 2.8.

The BF cost function penalizes the biarticular muscles acting between the hip and the knee, since factor α_2 is higher than the others. Figure 2.7 shows the knee moment (positive in extension) and all the obtained muscle forces acting at the knee. The forces exerted by the RF and HA obtained using the BF cost function were lower than those obtained with the EW cost function).

The results obtained with both cost functions are consistent with the constraints of the optimization problem equation (2.7), since the extensors (RF and VA) were activated when the extension moment was positive, and the flexor (HA) was activated when the extension moment was negative. There was co-contraction of antagonistic muscles. The GA (a knee flexor) was activated at the end of the stance phase of the injured leg, when the knee extensor moment was positive. This occurred because the GA is a biarticular muscle acting also at the ankle during the plantar flexion (see the ankle moment of the injured leg in Figure 2.5).

The muscle activations were calculated from the muscle forces obtained in the two-step optimization. The comparison between the muscle activations, calculated using the two cost functions mentioned above, and the normalized EMG data are shown in Figure 2.8. The plots show that the muscle activations were closer to the normalized EMG for the case of the cost function giving a lower *CFA*. The TA activation is the one showing a higher deviation from the corresponding EMG. This could be a consequence of an MVC value lower than the

physiological one (due to experimental errors) or of the difficulty in measuring the real activation due to the presence of connective tissue between the muscle and the electrode.

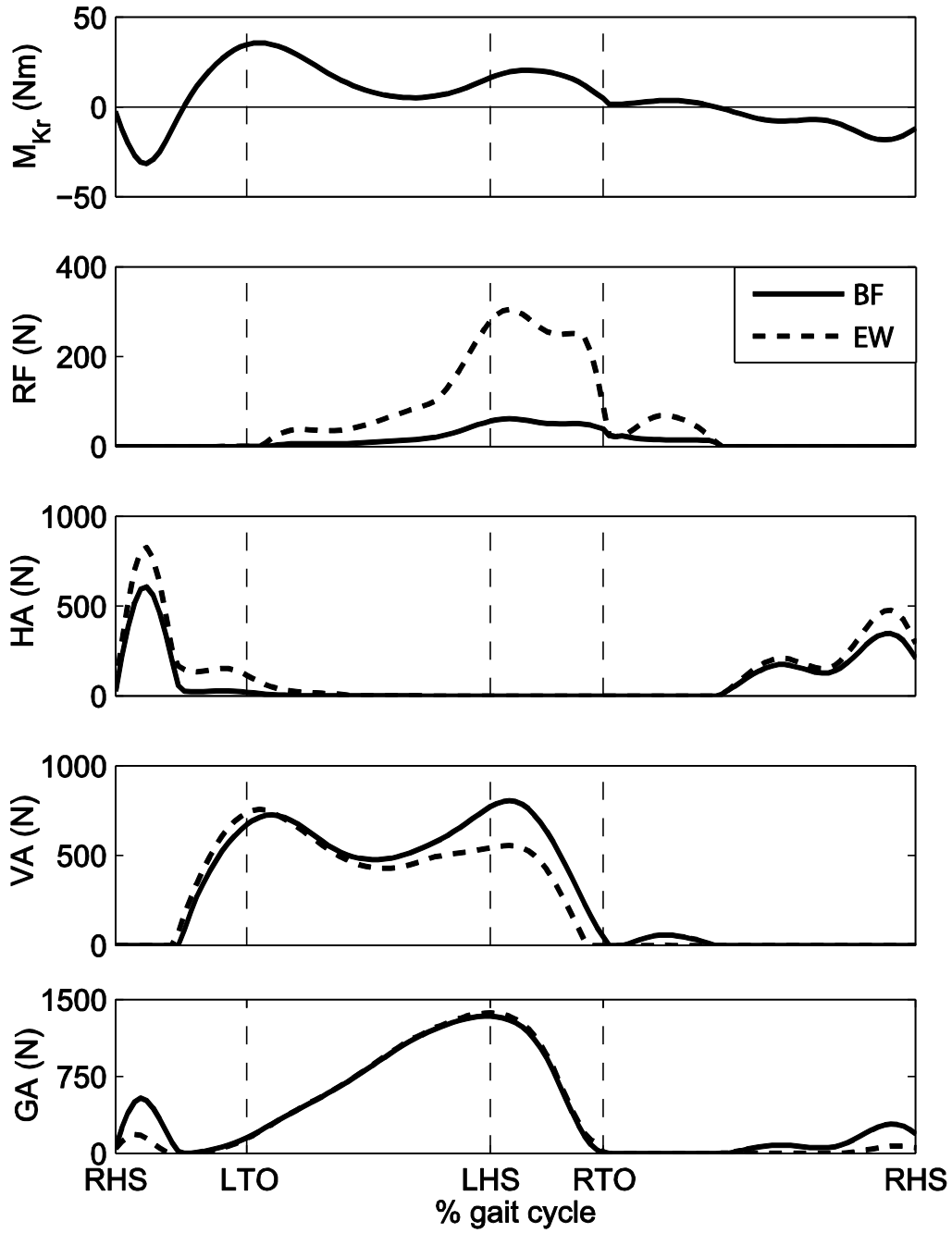

Figure 2.7. Right knee moment (in extension for positives values) and the forces of the muscles acting at the right knee for the BF cost function and the EW cost function.

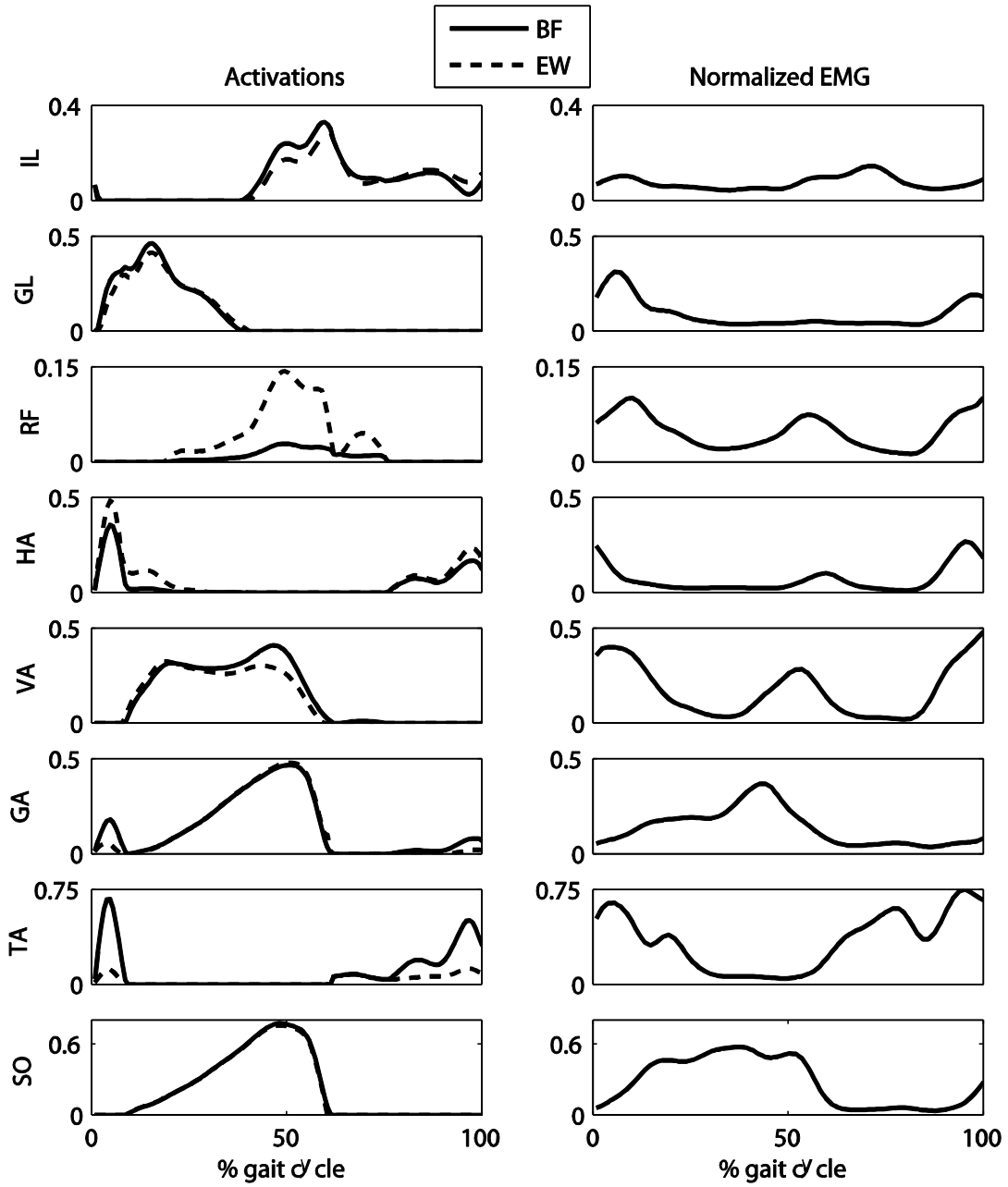

Figure 2.8. Activations of the muscles acting at the right knee for the BF and EW cost functions and the normalized EMG.

2.3.5 Analysis of the cost functions

The BF cost function penalizes the biarticular muscles acting between the hip and the knee (RF and HA). In Figure 2.9 the cost function terms $\left(J_K^m, J_K^{bp}, J_K^{bd}, J_{noK}\right)$ are compared. Figure 2.9(a) shows the optimization results using the BF cost function and Figure 2.9(b) that using the EW cost function. The differences are clear mainly at the beginning (0-10% cycle) and at the end of the stance phase (40-60% cycle), that is, when the J_K^{bp} value is lower using the

BF cost function. With this cost function the J_{noK} values were higher while J_K^{bd} values were lower. Although the increase of J_{noK} was high, the effect in the cost function J_{CNS} was low because its weighting factor was 0.1 instead of 0.25 (EW cost function). As shown in Figure 2.10, the total value of J_{CNS} is lower for the BF cost function during most of the cycle.

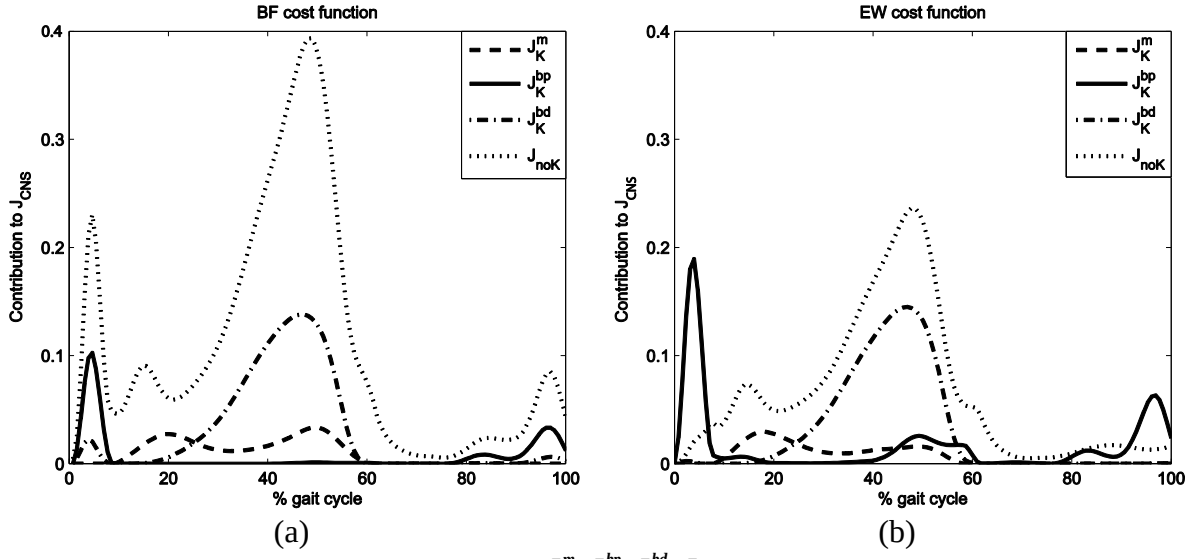

Figure 2.9. Components of the cost function $J_K^m, J_K^{bp}, J_K^{bd}, J_{noK}$ during the gait cycle for the BF cost function (a) and the EW cost function (b).

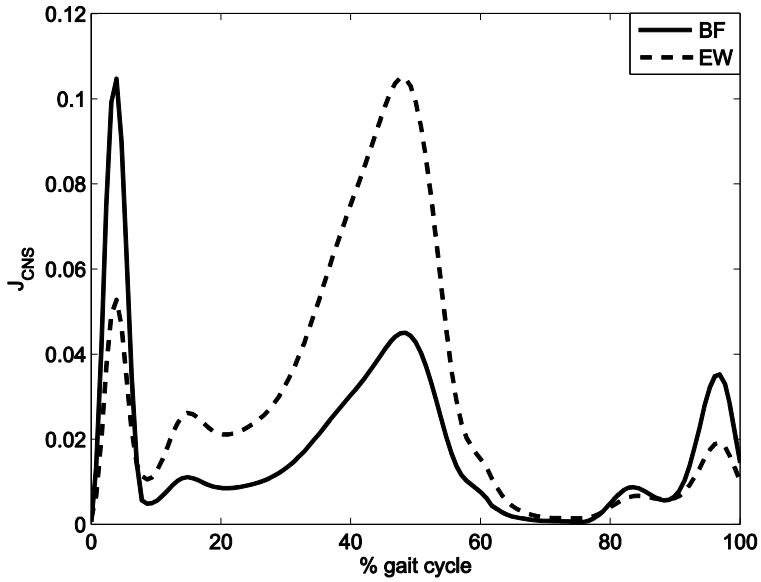

Figure 2.10. Values of the J_{CNS} for the BF and EW cost functions.

2.4 Conclusion

The main purpose of this study has been to investigate a consistent strategy followed by the CNS of a single injured subject (in this case suffering ACL rupture) to activate the muscles. Two novel contributions have been introduced in this study. The main original contribution is the use of a novel cost function where all muscles are not weighted equally. The muscles are grouped in four sets according to a physiological criterion (monoarticular on the injured joint, biarticular-distal, biarticular-proximal and other muscles). This has led to the simulation of 85 optimization problems. Another original contribution is the use of a two-step optimization method to have a higher probability that a global optimum is found when solving the muscle force sharing problem. The global algorithm CMA-ES gets closer to the minimum and the deterministic algorithm *fmincon* is used to reach the optimal muscle forces from a good initial estimate.

Slight alterations at the level of both joint kinematics and dynamics at the injured leg have been observed which are consistent with the literature studies. A decrease of the knee moment at the injured leg has been detected, which is due to the fact that the contribution to the total support is transferred from the knee to the ankle to avoid knee instabilities.

It has been observed that the strategy to activate the muscles which is more consistent with EMG measurements is different from the one that would be followed by a subject that weights equally all muscles. The cost function leading to more realistic muscle activations for our particular subject is the one that penalizes the biarticular muscles acting between the hip and the knee (RF and HA). This is in agreement with the hypothesis that the CNS does not weight all muscles equally.

In this study, the optimization formulation based on uniform muscle weightings, i.e. with equally weighted cost function, was associated to healthy subjects since this is the standard approach used in the literature. A further analysis could also have been carried out on healthy individuals to investigate whether or not the equally weighted cost function better fitted predicted muscle activations with normalized EMG compared to a non-uniform weighted cost function, as it was done in the study developed by Botasso et al. [33]. Another limitation is due to the simplicity of the model. As a result of the ACL rupture, the subject can experience small anterior translations between the tibia and the femur and we did not take them into account, since the knee was modeled as a hinge joint (one degree of freedom).

We did that simplification since with the motion capture system used in this work, it is not possible to measure these small relative translations. For this reason, we locked the degree of freedom related to the knee anterior-posterior translation and we assumed that not measuring that translation would not have a great effect neither on the calculation of the knee flexion moment through inverse dynamics nor on the calculation of moment arms.

This case study has been based on the kinematic and dynamic data of only one injured subject. The presented methodology to investigate the strategy followed by the CNS to activate the muscles could be also extended to other subjects suffering the same injury or even other joint injuries.

Chapter 3

Analysis of the activation - deactivation patterns and muscle synergies in ACL-deficient subjects during gait

3.1. Background

During human motion, it is believed that muscles are activated synergistically following a certain pattern depending on the motor task [34–37], that is to say, our central nervous system (CNS) does not activate the muscles independently. Muscle synergies are represented by modules consisting of one neural command (NC), which represents the time activation of a set of muscles, and one synergy vector (SV), which represents the weighting factor of each muscle to its NC. The number of NCs is lower than the number of muscles. Several algorithms have been used in order to calculate the muscle synergy components. The most widely used is the non-negative matrix factorization (NNMF), which ensures that NCs and SVs are both positive, while it minimizes the error between the reconstructed and the original signals [38,39].

It is believed that the number of synergies used by a human being when walking is between 4 and 6 [40–45]. The variance accounted for (*VAF*) between the reconstructed and the original signals is evaluated to select the proper number of modules to be used when factorizing the signals. Most authors consider that a $VAF>0.9$ is the threshold to accept the reconstruction [40,45]. It is reported that there are similarities in the muscle synergies when performing the same movement across subjects. Several authors reported muscle synergies when walking [40,41,45–47], walking with perturbations [44] or performing other tasks [48].

Clark et al. [40] applied the muscle synergy analysis in post-stroke injured subjects. They observed that, although the patterns were similar among groups, the complexity in post-stroke injured subjects was lower than in healthy subjects, i.e., they needed fewer modules to have a good signal reconstruction. It is unclear what synergistic strategy is followed by joint-injured subjects to activate the muscles spanning that joint. Depending on the joint injury, subjects can apply different activation strategies in order to avoid pain or to stabilize the joint.

Apart from the clinical evaluation of muscle co-contraction, the use of the factorization can be useful for motion analysis and simulation. There is indeterminacy when calculating the muscle forces, since they cannot be measured experimentally due to invasiveness. The usual method to estimate the forces is with the resolution of an optimization problem [49], which consists of minimizing a cost function (a physiological variable) that represents the strategy of the CNS to activate the muscles. The optimization results can produce multiple physiologically feasible solutions due to the muscle redundancy. Some authors used the muscle synergy components in order to decrease the indeterminacy in the muscle force calculations, either in forward dynamics [43,46] or inverse dynamics [50] approaches. Regarding ACL-deficient subjects, differences have been observed at the joint level as well as at individual EMG signals [1,51–53]. As far as the authors know, the muscle synergy analysis has not been applied yet to subjects with this kind of injury. In consideration of that, this study could be useful at two levels. On the one hand, in a clinical application it would allow the specialist to follow the rehabilitation process of injured subjects. On the other hand, in a motion dynamic analysis, muscle synergies could be used to decrease the indeterminacy in the muscle force calculation of ACL-deficient subjects.

In this study, we evaluated and compared the EMG patterns in healthy and injured subjects when walking. EMG data were collected from both legs at the same time in order to avoid the variability that could appear when data are obtained from different gait trials. According to the well-known classification of ACL-deficient subjects, it is considered that they can be divided in three groups [54]: copers, who return to the preinjury level of their daily tasks and sport activities; non-copers, who cannot return to their preinjury level of tasks and sport activities and have episodes of full giving way even in daily tasks; and adapters, who reduce

or modify certain tasks or the sport level to prevent their knee giving way. In our study, all ACL-deficient subjects were considered adapters and the measures were done a few days or weeks before the surgery of the ligament reconstruction. Although muscle synergy patterns can present many similarities among groups, since all of them perform the same task, human gait, our hypothesis was that the pattern of muscle synergy components may have different tendencies. As mentioned, there are studies that evaluate individual muscle activations in ACL-deficient subjects, but the objective of this study is to evaluate the differences in muscle synergies compared to healthy subjects in order to better understand the muscle activation pattern in absence of ACL function. The analysis comprises two steps. The first is a comparison of the activation-deactivation pattern among healthy legs (Control group), injured subjects' injured legs (Ipsilateral group) and injured subjects' non-injured legs (Contralateral group). Then, a muscle synergy analysis is reported and compared among the three groups.

3.2. Methods

3.2.1. Subjects

Ten healthy subjects, five men and five women (age 31.5±12.9 years), and eighteen ACL-deficient subjects, twelve men and six women (age 32.3±10.99 years), volunteered as participants in this study. No healthy subjects suffered any lower-limb injury. The injured subjects were classified as adapters, according to the medical staff and the widely used classification presented in [54]. All injured subjects reported that they could deal with daily live and they did not suffer pain when normal walking, however, they felt discomfort and pain when they did sports that required knee pivoting, such as football or skiing. The time interval from the injury varied from one month to three years (10.3±12.0 months). All subjects provided their consent to contribute to this study.

3.2.2. Experimental setup

All volunteers were asked to walk a minimum of three overground gait cycles at a self-selected speed (0.77±0.12 m/s healthy subjects and 0.80±0.13 m/s injured subjects). One of the gait cycles was selected from the recorded trials and was analyzed.

EMG data from sixteen muscles were measured with sixteen surface EMG sensors (Biometrics, Newport, United Kingdom) at 1000 Hz. The signal of eight lower-limb muscles from each leg of the subjects was measured (Tibialis Anterior –TA–, Soleus –SO–, Gastrocnemius Lateralis –GL–, Gluteus Maximus –GM–, Rectus Femoris –RF–, Vastus Lateralis –VL–, Semitendinosus –ST– and Extensor Digitorus Longus –ED–). The EMG data for each subject (right and left leg) came from the same gait trial, which decreases the variability due to the differences that could appear when measuring different gait trials separately.

EMG signals were demeaned, rectified and filtered with a Butterworth low-pass filter at 6 Hz. Then, they were normalized by maximum voluntary contraction (MVC) values obtained by MVC exercises previously done. The exercises were selected in order to calculate the maximum muscle excitations [55]. The volunteers were asked to apply force against a resistance along a direction to activate the muscles responsible for: ankle plantar flexion/dorsiflexion (ED, SO, TA, GL), knee flexion/extension and abduction/adduction (RF, ST and VL) and hip flexion/extension and abduction/adduction (GM, ST and RF). Data from these trials were processed in the same way that walking trials (demeaned, rectified and filtered at 6 Hz). The maximum values of EMG were selected among all available trials (MVC exercises and gait trials). These values were verified visually and individually in each subject in order to avoid the acceptance of a wrong maximum value. All MVC exercises, as well as verifications, were carried out by the same technician in order to standardize the comparison. Using this normalization, the signal was constrained to be between 0 (not activated) and 1 (maximum activation). So, an activation close to 1 would mean that the muscle is near to its maximum activation.

Ground reaction forces (GRF) and marker trajectories were also measured to identify the events of the gait cycle. The GRF were measured by means of two force plates (AMTI, Watertown, MA) at 100 Hz. Two marker trajectories from each foot (heel and tip of the first metatarsal bone) were captured by fourteen infrared cameras (Naturalpoint, Corvallis, OR). Once the gait cycle was identified for each leg, data was interpolated to 101 frames. EMG, GRF and marker trajectories will be available on the net.

3.2.3. Data Analysis

Data analysis was carried out by means of Matlab (Mathworks, Natick, MA) and using the Parallel Computing Toolbox to decompose the signals. All data were divided in three groups: Control, which consists of data from healthy subjects; Ipsilateral, from the ipsilateral leg, which is affected by the ACL injury; and Contralateral, from the non-injured leg of the ACL-deficient subjects.

Activation-deactivation pattern

An initial analysis of the activation-deactivation pattern for each muscle was carried out to identify the differences in the activation timing between groups. The on-off activation pattern was calculated for each subject, considering EMG signal to be activated when it was higher than the following threshold:

$$Threshold_{on-off} = \min\left(EMG\right) + 0.5\left(\max\left(EMG\right) - \min\left(EMG\right)\right) \tag{3.1}$$

where EMG stands for an EMG signal. The activation pattern was calculated for each group. A muscle was considered to be active when more than 50% of the subjects had this muscle activated at a particular time frame.

Non-negative matrix factorization

EMG processed signals were factorized applying the non-negative matrix factorization (NNMF) to obtain the muscle synergy components: neural commands (NCs) and synergy vectors (SVs) [39]. The factorization consists of decomposing the matrix containing all EMG signals (*nframes* x *nmuscles*) by two matrices: the NCs, which represent time activation of each module (*nframes* x *nmodules*) and SVs, which contain the weights of each muscle to each module (*nmodules* x *nmuscles*). The algorithm to decompose the signal was based on the non-linear least square algorithm (*lsqnonlin*), which minimizes the error between the reconstructed and the experimental EMG signals at each iteration step [50]. The maximum value of each SV was constrained to be 1 in order to decrease the indeterminacy of the factorization. The NNMF was applied six times per trial, decomposing the signal in 1 to 6 modules.

Comparison of results

The match of the reconstructed EMG with the experimental one was evaluated by means of the variance accounted for (*VAF*) value, calculated as follows:

$$VAF = 1 - \frac{\sum_{t=1}^{101} EMG_t^{rec} - EMG_t^{exp}}{\sum_{t=1}^{101} EMG_t^{exp}} \tag{3.2}$$

where EMG_t^{rec} and $EMG_t^{\exp}$ stand for the reconstructed and the experimental EMG signals at frame *t* respectively. In order to compare statistically whether two values from two different samples were different (such as the comparison of *VAF* values), a t-test analysis was carried out and a p-value was calculated. If p-value<0.05, then the values were considered to be statistically different.

The differences in the tendency of SVs and NCs were measured by means of the Pearson's correlation coefficient [40]. If this value was close to 1, it meant that the shape of the compared sets of data was similar. In order to identify whether two NCs or SVs were statistically correlated, the threshold of the p-value was set equal to 0.001.

3.3 Results

3.3.1 Activation-deactivation pattern

Figure 3.1 shows the activation-deactivation pattern of the eight analyzed muscles for the three data groups. It is remarkable that Ipsilateral and Contralateral TA showed a longer activation during the early stance phase (0-40%). Moreover, the Ipsilateral's TA was active during all swing phase whereas Control's and Contralateral's TA activation just appeared in the beginning and at the end of this phase. SO and GL were only activated during the stance phase and both were activated earlier in Ipsilateral and Contralateral groups. GM activation was slightly longer in the ipsilateral leg. Regarding the knee muscles, it can be observed that the co-contraction of the injured subjects' quadriceps (RF and VL) and hamstrings (ST) was longer during the stance phase. Finally, Ipsilateral's ED activation pattern was slightly different from the other two groups, since both activation and deactivation of the injured subjects' ED appeared earlier than in the other two groups.

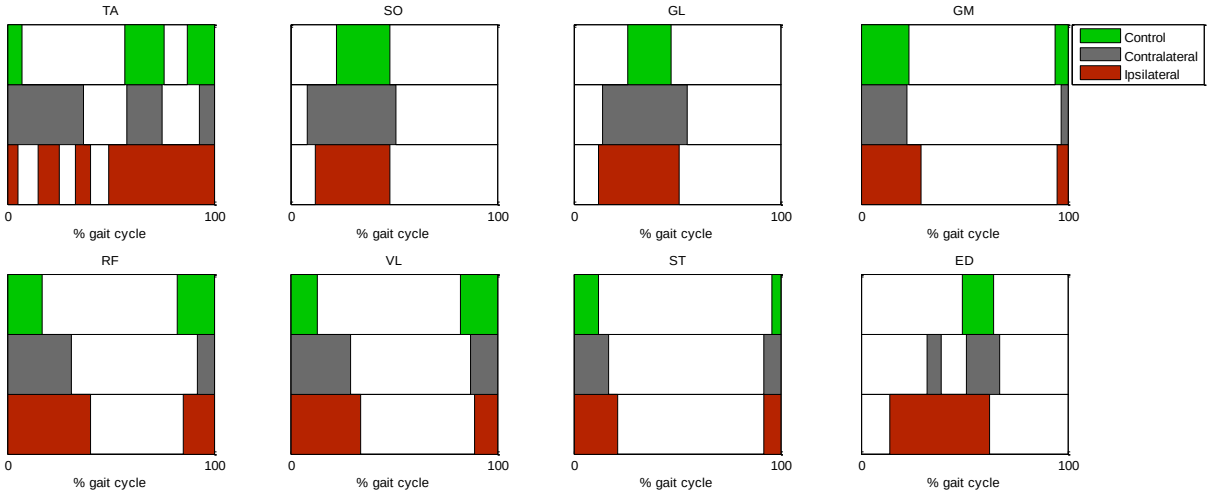

Figure 3.1. Muscle activation-deactivation patterns during gait cycle for the three groups: Control, Ipsilateral and Contralateral.

3.3.2 Analysis of dimensionality

The similarity between the experimental and the reconstructed EMG signals was measured using the *VAF* value. The t-tests to compare the *VAF* values of the three groups showed that there were no significant differences in the dimensionality among groups, neither using 4 modules (p=0.20 Control vs. Ipsilateral, p=0.15 Control vs. Contralateral and *p=0.82* Ipsilateral vs. Contralateral) nor 5 modules (p=0.96 Control vs. Ipsilateral, *p=0.82* Control vs. Contralateral and p=0.69 Ipsilateral vs. Contralateral). Control group had a higher *VAF* in some muscles (such as GL, ST and ED when using 5 modules) and, in other muscles (such as GM and VL when using 5 modules) injured subjects had a higher *VAF*.

The reconstructed EMG signal reproduced the experimental one with a mean *VAF* value higher than 0.8 for all eight muscles using 4 modules (Figure 3.2). However, VL and ST signals were reconstructed with a mean *VAF*<0.9. The use of a fifth module increases all *VAF* values, and in this case, the values of *VAF* were higher than 0.9 in all muscles. Therefore, in this study, 5 motor modules (synergies) were selected to compare the modules among groups.

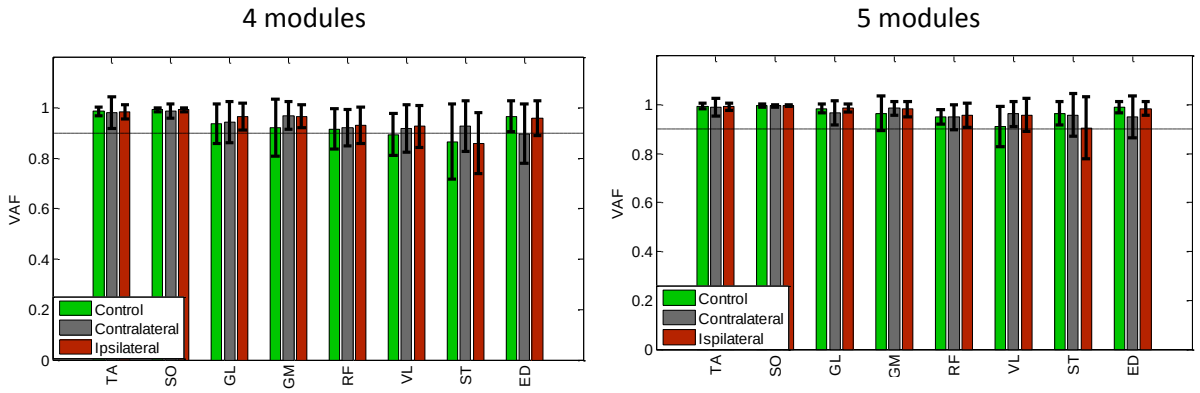

Figure 3.2. Mean *VAF* values of all muscles using 4 (left) and 5 modules (right). Black vertical lines represent 1 standard deviation from the mean values. Horizontal dashed black line stands for the threshold of *VAF*=0.9.

Three common modules were observed when decomposing EMG signals with 4 and 5 modules. Figures 3.3 and 3.4 show NCs and SVs of the Control group (right and left leg). In both cases there were 3 common modules. Module 2 basically consisted of SO and GL activity. Module 3 mainly consisted of TA activity, since the SV for this muscle was 1 for most subjects. For some subjects this module also had GM and ST activity. ED was the main contributor to module 4 in Figure 3.3. All these three modules can be observed when using 5 modules to decompose the signal (Figure 3.4). When decomposing the signal with 4 modules (Figure 3.3), module 1 consisted of a mix of muscle activations, the most representatives were GM and ST, but quadriceps (RF and VL) activations were also present in most subjects. This module was divided into two when decomposing the signal with an additional module (shown as module 1 and 4 in Figure 3.4). In this case, module 1 basically consisted of GM activation and module 4 mainly consisted of ST activation, although GM also had an important contribution in several subjects.

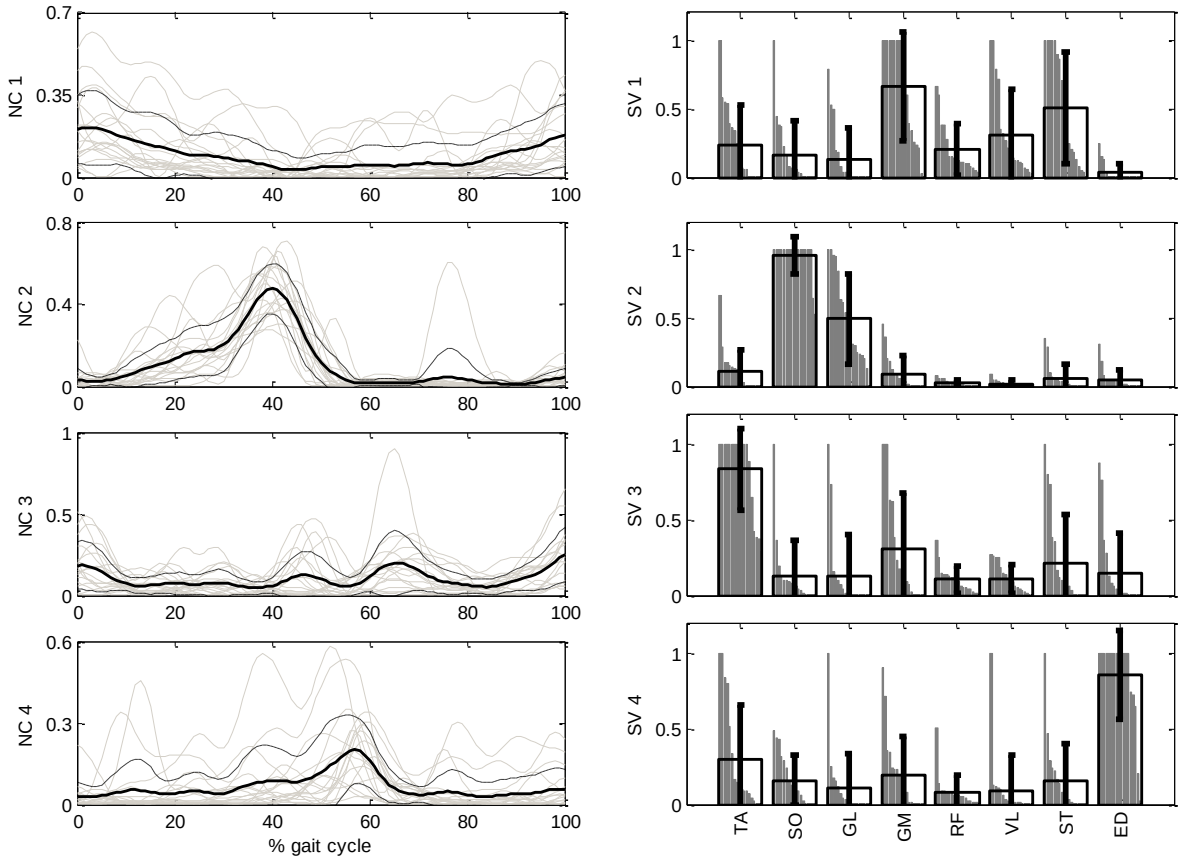

Figure 3.3. Synergy components from Control group decomposing EMG signals in 4 modules. NCs for all subjects (in grey, left) with their mean values (thick black lines) and standard deviations (dashed lines). SVs for all subjects in descend order (in grey, right) with their mean values (in black bars) and standard deviations (in error black bars).

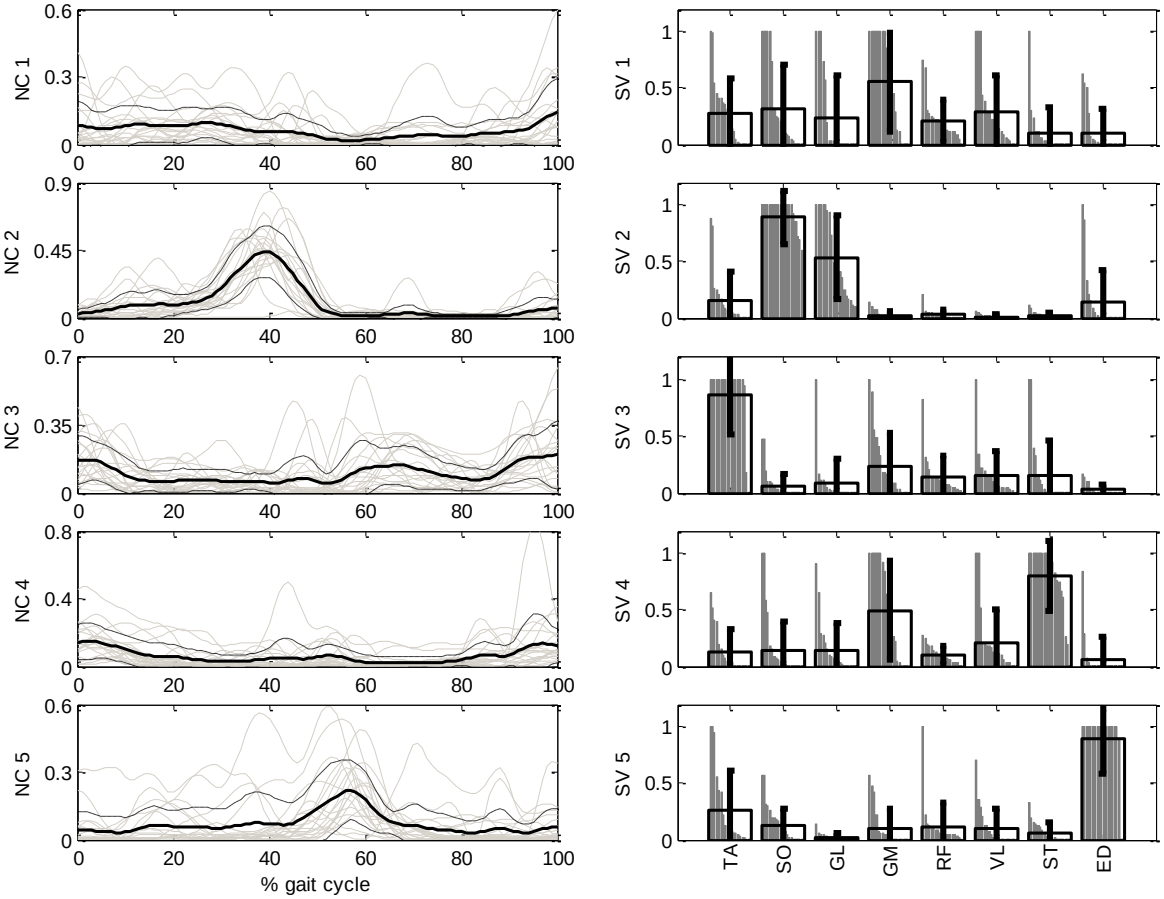

Figure 3.4. Synergy components from Control group decomposing EMG signals in 5 modules. NCs for all subjects (in grey, left) with their mean values (thick black lines) and standard deviations (dashed lines). SVs for all subjects in descend order (in grey, right) with their mean values (in black bars) and standard deviations (in error black bars).

3.3.3 Variability intra-groups

The number of modules was fixed to 5 and the correlation of the NCs and SVs between modules was analyzed within each group as in [40]. Table 3.1 shows that the correlation among modules within each group was overall low, what means that the SVs and the NCs of the modules were independent from each other.

However, there were some slight similarities (significant positive correlations) in the shape of the NCs between modules 3 and 4, and modules 1 and 4 in the Control group (r=0.58 and r=0.52 respectively); between modules 1 and 3, and modules 1 and 4 in the Ipsilateral group (r=0.34 and r=0.56 respectively); as well as between modules 1 and 3, 1 and 4, in the Contralateral group (r=0.37 and r=0.82 respectively).

Table 3.1. Correlation of the mean NC curves and SV values among modules for all three groups.

Control

NC

	1	2	3	4
2	0.20			
3	0.16	-0.48		
4	**0.52**	-0.21	**0.58**	
5	-0.58	-0.06	-0.19	-0.34

SV

	1	2	3	4
2	0.05			
3	0.18	-0.23		
4	0.06	-0.36	-0.05	
5	-0.38	-0.13	-0.07	-0.38

Ispilateral

NC

	1	2	3	4
2	0.05			
3	**0.34**	-0.59		
4	**0.56**	-0.26	0.30	
5	-0.5	-0.31	0.29	-0.14

SV

	1	2	3	4
2	-0.26			
3	-0.23	-0.10		
4	0.03	-0.59	0.14	
5	-0.26	-0.31	-0.17	-0.41

Contralateral

NC

	1	2	3	4
2	0.04			
3	**0.37**	-0.33		
4	**0.82**	-0.29	0.18	
5	-0.43	-0.12	-0.11	-0.26

SV

	1	2	3	4
2	-0.16			
3	0.20	-0.14		
4	-0.09	-0.40	-0.26	
5	-0.09	-0.09	0.22	-0.58

Bold values indicate that there is significant positive correlation (p-value<0.001)

3.3.4 Variability inter-groups

Figures 3.5 to 3.7 show the comparison between NCs and SVs from two groups (Control vs. Ipsilateral, Control vs. Contralateral and Ipsilateral vs. Contralateral, respectively). Although the tendencies of SVs and NCs were similar in all groups, there were some differences that were quantified in Table 3.2 through Pearson's correlation coefficients.

The comparison of all SVs from the same module between Control and Ipsilateral groups shows that they follow the same trend. However, in modules 1 and 4, the *r* values were lower than 0.9 (Table 3.2). In module 4, the mean TA and RF components of the SV were significantly higher in the Ipsilateral group (p=0.03 and p=0.01 respectively). It is also observed that during the stance phase in module 3 (basically TA activation), the NC was lower in the Control group (r=0.69). A similar result was obtained in module 1 (r=0.77).

There were no significant differences in the pattern of SV between the Control and the Contralateral groups (r>0.9 in all modules), but there were differences in the NCs. The shape of the third NC of the Contralateral group was quite different from the Control group

(r=0.43). Like in the Ipsilateral group, modules 1 and 3 of the Contralateral group were higher than those of the Control group at the early beginning of the stance phase.

Mean SV values between the ipsilateral and contralateral legs were well correlated, except in module 1, in which r=0.77. The main significant difference was in the mean TA component of the SV (p=0.001). The correlations of the third and fourth NC between these two groups were low (r=0.49 and r=0.69 respectively). The main differences were during the beginning of the stance phase (0-20% of the cycle) and at the transition to the swing phase (50-65% of the cycle). There was also a difference in the fifth NC (r=0.72). The activation of the ED was lower in the contralateral leg than in the ipsilateral leg at the transition between the stance and the swing phase (~60% of the gait cycle).

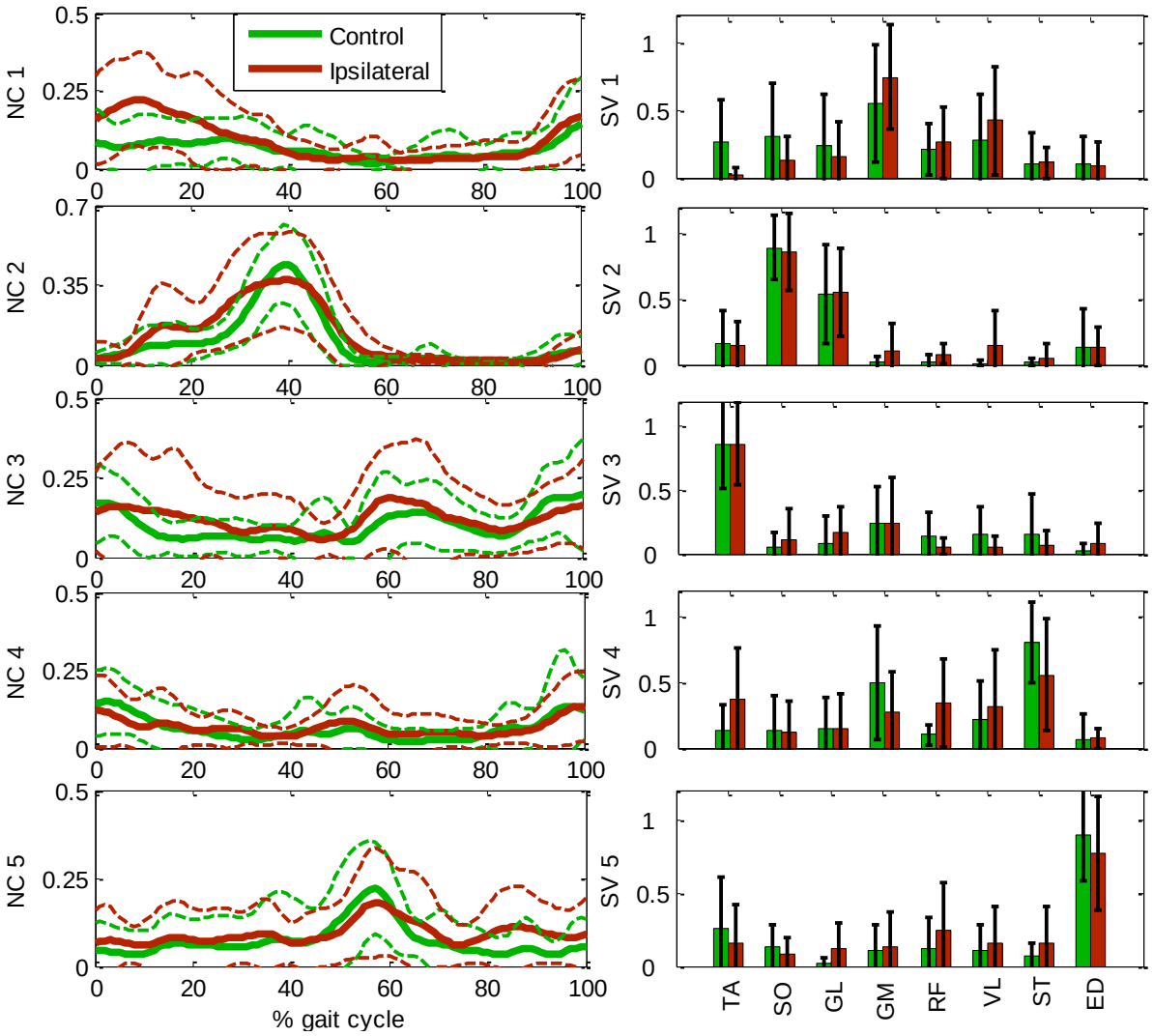

Figure 3.5. NCs (left) and SVs (right) for Control and Ipsilateral groups. The thick lines in the left plots represent the mean value of the NCs and dashed lines ± 1 standard deviation. In the right plots, the bars represent the mean value of the SVs for all subjects and the black error bars their standard deviations.

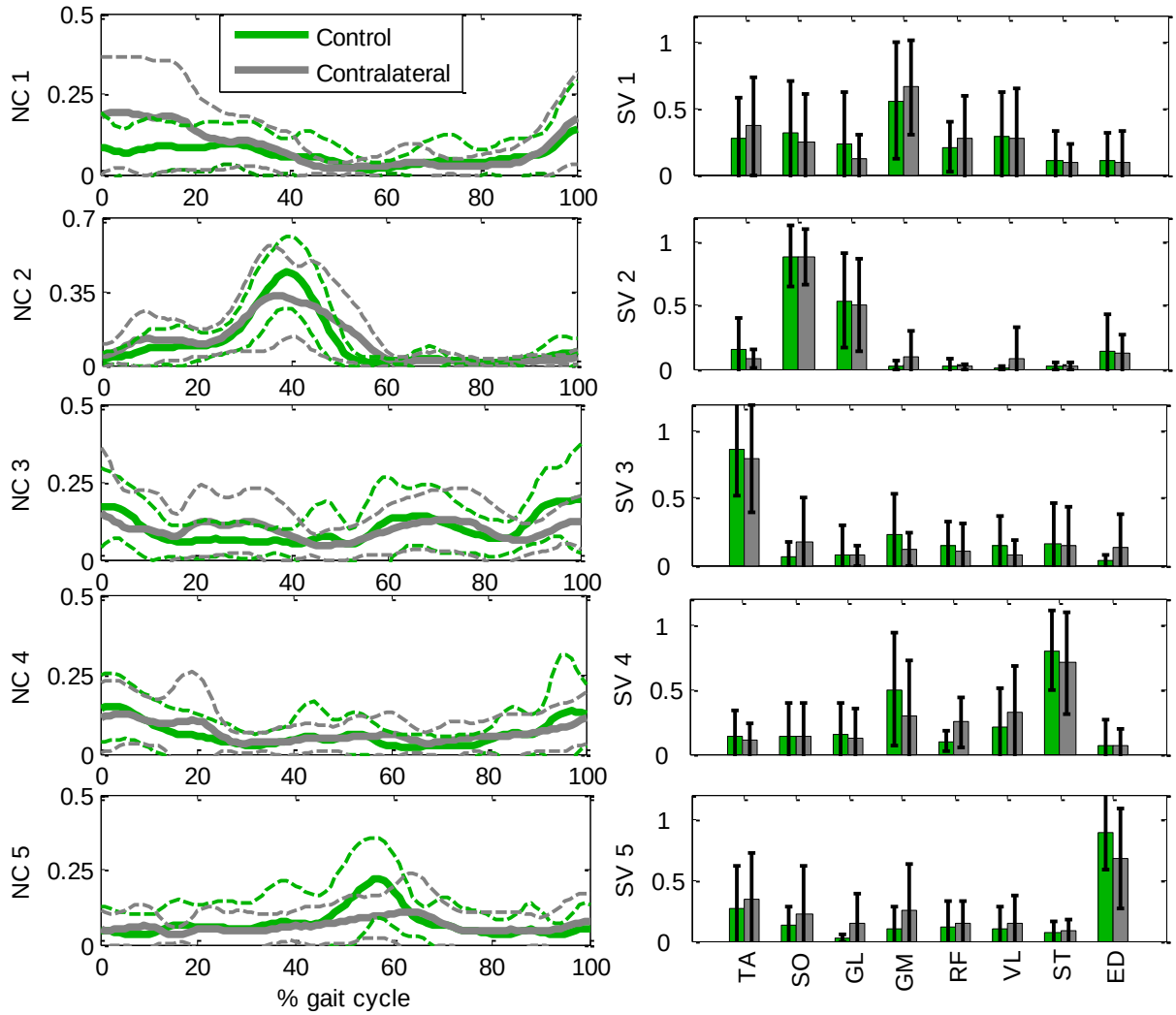

Figure 3.6. NCs and SVs for Control and Contralateral groups. Refer to Figure 3.5 for meaning of thick and dashed lines as well as the error bars.

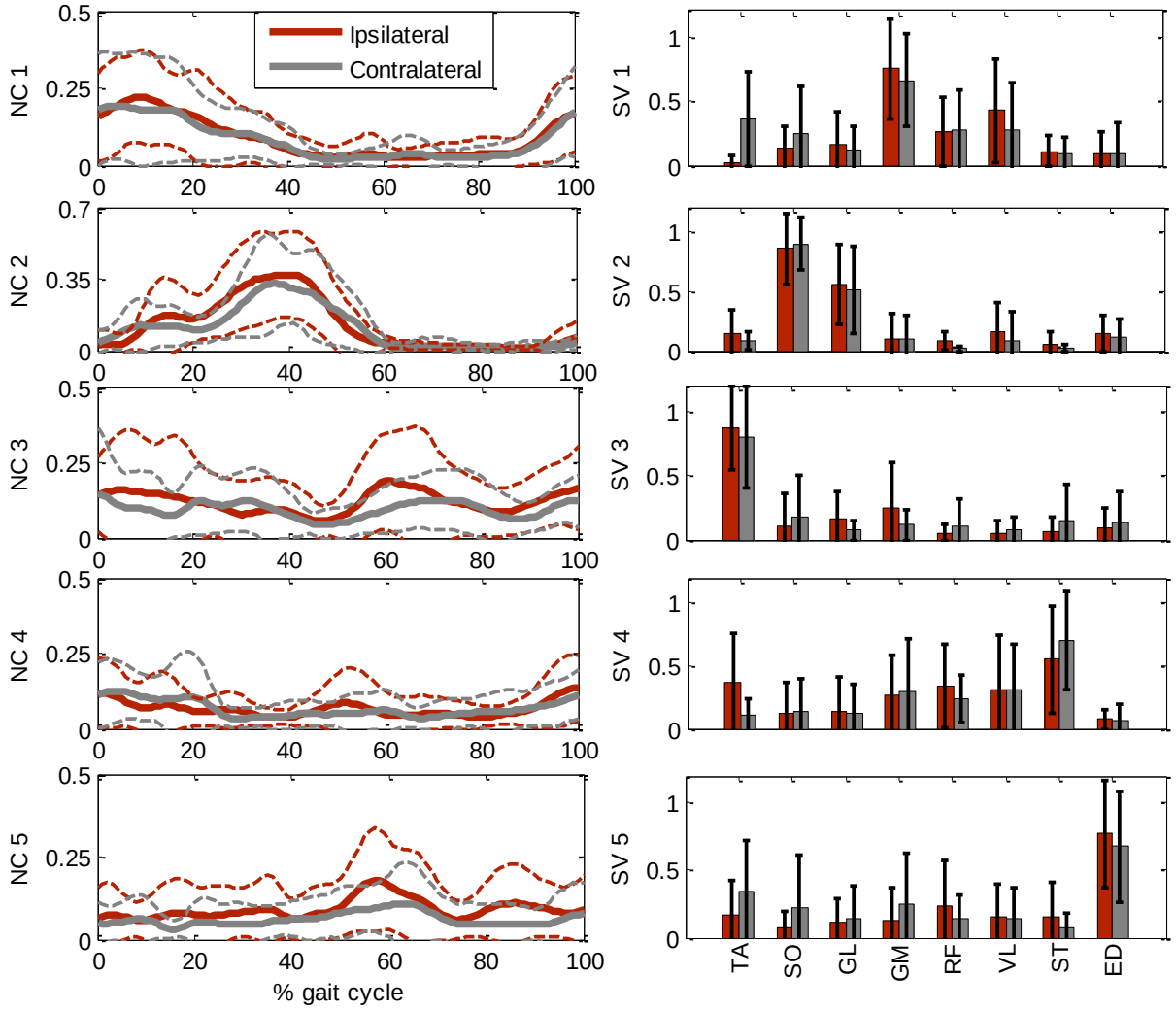

Figure 3.7. NCs and SVs for Ipsilateral and Contralateral groups. Refer to Figure 3.5 for meaning of thick and dashed lines as well as the error bars.

Table 3.2. Correlation of the mean NC curves and SV values among modules and groups.

NC

Control / Ipsilat.	1	2	3	4	5
1	**0.77**				
2	-0.04	**0.94**			
3	0.19	-0.63	**0.69**		
4	**0.69**	-0.28	0.30	**0.86**	
5	-0.42	0.01	0.11	-0.07	**0.81**

SV

Control / Ipsilat.	1	2	3	4	5
1	0.80				
2	-0.36	**0.99**			
3	-0.18	-0.28	**0.96**		
4	0.28	-0.35	-0.17	0.70	
5	-0.32	-0.20	0.03	-0.47	**0.96**

NC

Control / Contralat.	1	2	3	4	5
1	**0.79**				
2	0.01	**0.92**			
3	0.24	-0.62	**0.43**		
4	**0.70**	-0.20	0.08	**0.84**	
5	-0.44	0.12	-0.36	-0.30	**0.73**

SV

Control / Contralat.	1	2	3	4	5
1	**0.93**				
2	-0.22	**0.99**			
3	0.38	-0.31	**0.95**		
4	0.10	-0.31	-0.17	0.91	
5	-0.28	-0.17	0.10	-0.43	**0.96**

NC

Contralat. \ Ipsilat.	1	2	3	4	5
1	**0.98**				
2	0.08	**0.96**			
3	**0.36**	-0.60	**0.49**		
4	**0.59**	-0.19	0.10	**0.69**	
5	-0.50	-0.25	-0.26	-0.31	**0.72**

SV

Contralat. \ Ipsilat.	1	2	3	4	5
1	0.77				
2	-0.19	**0.99**			
3	0.36	-0.13	**0.96**		
4	0.07	-0.60	0.23	0.82	
5	-0.38	-0.28	-0.10	-0.32	0.87

Bold values indicate that there is significant positive correlation (p-value<0.001)

3.4 Discussion

This study deals with the investigation of the differences in the muscle activation patterns between healthy subjects (Control group) and ACL-deficient subjects (Ipsilateral and Contralateral groups). The differences were studied at two levels: individual muscle timing patterns and muscle synergies. As far as the authors know, no previous study was carried out calculating the muscle synergy components in ACL-deficient subjects.

Courtney et al. [56] reported the onset and offset patterns of the Tibialis Anterior, Gastrocnemius Medialis, Medial Hamstrings and Quadriceps during fast-inclined walking in a treadmill for a Control group and an Adapter ACL-deficient group. Authors found that Tibialis Anterior and Medial Hamstrings had a longer activation period, which is in agreement with the presented results for the TA and ST muscles. They did not observe differences in Quadriceps (represented by RF in our study). Gastrocnemius Medialis pattern of the Adapter group (activated just before and after the heel strike) was different compared to results obtained for the Ipsilateral and Contralateral GL (mainly activated during the mid stance phase). Nevertheless, this difference could be attributed to the fact that the gait was faster than in our study and there was an inclination.

Knoll et al. [52] studied the gait adaptations at the level of muscle activations of ACL-deficient subjects before and after the surgery. They measured EMG signals in Vastus Lateralis and Medialis, Adductor Longus and Biceps Femoris during walking. The activation-deactivation patterns obtained in their study are comparable to the ones in Figure 3.1. Overall, Ipsilateral's VL and Biceps Femoris had a longer activation. In the work presented here, the results of the Biceps Femoris activation pattern are comparable to the ST pattern, which also belongs to Hamstrings. These results show longer co-contraction between Hamstrings and Quadriceps to stabilize the knee joint.

These results are in agreement with the fact that both muscles, Hamstrings (knee flexor) and Quadriceps (knee extensor), are stabilizing the knee when the ACL is ruptured [51,57]. These muscles control the joint in order to avoid high displacements of the tibia with respect to the femur. There were also observable differences in muscles which control the ankle (SO, TA, GL and ED). The activation of these muscles was longer for the ACL-deficient subjects. As Chmielewski et al. [57] mentioned, there is a shift of support moment from the knee to the ankle what may suggest that there is a transfer of the leg control away from the injury.

There were no statistical differences regarding the dimensionality of the signal factorization. In this case there were no observable differences in the number of modules needed to reconstruct the signals among groups, which represents that the control of the CNS is not more complex in ACL-deficient than in healthy subjects, in contrast with other studies which analyzed post-stroke subjects [40]. The *VAF* values that evaluated the reconstruction of the EMG signal were similar, either using 4 or 5 modules. These results showed that the pattern of the EMG activity of the ACL-deficient subjects was not more complex than the one of the healthy subjects. However, this fact did not exclude that some differences could be detected between groups. Figure 3.2 showed that in all three groups, the *VAF* values of all muscles were higher than 0.9 using 5 modules, so the muscle synergy analysis was carried out using 5 synergies [40]. The analysis of the differences intra-groups showed that all modules were overall independent from each other.

EMG data were collected at both legs simultaneously. Measuring left and right legs at the same time avoided the differences that could appear when measuring the EMG in two different cycles. EMG was normalized by MVC values, what allowed comparing the differences in the magnitude of the NCs (time-dependent synergy components). In Figures 3.5 to 3.7, it can be observed that NCs 1, 3, 4 and 5 were overall comprised between 0 and 0.4 and NC 2 was slightly higher (comprised between 0 and 0.62).

NCs and SVs are comparable to other studies that analyzed the muscle synergy components in healthy subjects. Oliveira et al. [45] carried out a study to compare the influence of EMG processing (averaging, concatenation and the used number of cycles) in the muscle synergy factorization. They reported the results for 5 modules. Our first 4 modules can be identified

in 4 of their modules. The fifth module is different due to the fact that they did not measure ED signal (contained in module 5 in our case). Clark et al. [40] carried out a study of the muscle synergy analysis with paretic and healthy subjects and Neptune et al. [46] simulated gait using muscle activation modules. Both studies reported results for 4 modules that could be identified with our modules 1 to 4. They did not include ED in the muscle synergy analysis, which in our case participated in module 5. In all mentioned studies, EMG was normalized over all trials. In this study, EMG data were normalized by MVC values in order to evaluate differences in the magnitude of NCs.

Although the differences were small, SVs tended to be more similar between Control and Contralateral groups, suggesting that in those groups the CNS activates the same groups of muscles synergistically. However, it is not clear which groups presented comparable NCs. Modules 1 and 2 presented similar NCs between Contralateral and Control groups and modules 3 to 5 between Control and Ipsilateral groups. Therefore, the control of both legs of the injured subjects suffered small alterations compared to healthy subjects. Figures 3.5 to 3.7 show that the variability in the NCs among subjects was higher for the injured subjects (Contralateral and Ipsilateral group). However, some tendencies can be observed. The second NC (which activated mainly SO and GL) in the Ipsilateral group presented two peaks during the stance phase and the NCs of modules 1 and 3 were higher at the beginning of early stance compared with the Control group. This could be caused by the fact that the subject tried to stabilize the joints of the ipsilateral leg. In the same line of the observed results in the onset-offset patterns, Quadriceps and Hamstrings presented more co-contraction in the Ipsilateral group than in the Control one. In Figure 3.5, it can be observed that the fourth SV of the Ipsilateral group presented weights higher for the RF and VL (Quadriceps) and lower for the ST (Hamstrings) than in the Control group. This fact yielded similar Quadriceps and Hamstrings weights, indicating higher co-contraction at the knee. Figure 3.7 shows that the peak of the module 5 (mainly related to ED activation) at the transition between the stance to swing phase was higher for the Ipsilateral and Control group than for the Contralateral group. The explanation of this result in module 5 could be two-fold: either the control of the injured leg is transferred to the ankle, as mentioned in [57], which is suggested with the comparison of Ipsilateral and Contralateral groups (also

observed in onset-offset patterns); or the contralateral leg avoids providing a high acceleration to the body at toe off which would destabilize the injured leg during its initial stance, suggested by the smoother curve of the fifth NC of the contralateral leg compared to the one of the ipsilateral leg.

Three main limitations of our study should be recognized. The first one is that, although the identification of the differences from a Control group could be useful to observe objective improvements during a rehabilitation treatment (to reinforce the clinical evaluation), a post-surgery follow-up study should be carried out to see how the muscle synergy components change along time. Some studies in the literature mention that the EMG pattern restores to levels similar to prior the injury [52,58], but authors of these studies analyzed individual EMG signals and no synergy components. The second limitation is the sample size. With a wider sample, a study could be carried out to evaluate whether the ACL-deficient subjects suffer other injuries or not. Comparing the muscle synergies with the observed tendencies from an ACL-deficient population could be useful to detect anomalies. The third limitation is related to the use of only one gait cycle. Due to space limitations, we only analyzed one gait trial. As mentioned, some separated gait trials were performed over the force plates and we picked the one with the cleaner data. Processing more than one trial could reduce intra-groups variability yielding to more conclusive results.

In conclusion, our initial hypothesis was fulfilled. Despite the similarities among groups, different trends were identified. The analysis of these muscle synergy tendencies can be useful as a follow-up study during a rehabilitation treatment. Another important field of application is in motion simulation. Recently, some studies used muscle synergy components to decrease the indeterminacy when calculating the muscle forces in dynamic simulations of healthy subjects [43,46,50]. Using muscle synergy components extracted from ACL-deficient subjects could be also useful to predict muscle forces in gait dynamic analyses of those subjects.

Chapter 4

Two-step optimization problem formulation for predicting knee muscle and contact forces during gait

4.1. Background

Disorders affecting walking ability (e.g., osteoarthritis and stroke) are prevalent in society. Worldwide each year, approximately 15 million individuals suffer a stroke [59] and 250 million individuals are diagnosed with knee osteoarthritis [60]. Walking dysfunction from these and other disorders leads to a decreased quality of life and other serious health conditions such as heart disease and diabetes, thereby increasing the risk of death as well [61]. Unfortunately, current clinical interventions are largely ineffective at reversing walking impairments [62,63]. Even total joint replacement frequently does not achieve full normalization of walking function [64]. Improved clinical treatment methods are therefore needed to address this important society problem.

Researchers have begun to explore using computational walking models to develop improved clinical interventions for walking impairments [65]. One of the primary challenges with this approach is indeterminacy of model-predicted muscle forces, since more muscle actuators exist than degrees of freedom in the skeleton. Researchers have explored several computational approaches to address the muscle redundancy problem. The most common approach found in the literature is static optimization, where a cost function is minimized one time frame at a time to find muscle forces that reproduce experimental joint moments calculated via inverse dynamics [6,49,66,67]. Musculoskeletal models used in this process are typically scaled versions of generic models available in the literature [68,69]. While this

approach can be computationally efficient, it does not take advantage of experimental EMG data when available, and the correct physiological form of the cost function to be minimized is unknown. A growing alternate approach is to use an EMG-driven model whose muscle excitation inputs are taken directly from experimental EMG measurements [70–72]. With this approach, no assumptions are required about the form of the cost function being minimized, plus model parameter values are often calibrated to match the subject's experimental joint moments from inverse dynamics. However, "flexibility" still remains in the solution process, since the absolute amplitude of each muscle EMG signal is difficult to determine, the number of EMG measurements is often limited, and EMG data are typically unavailable from large deep muscles (e.g., psoas). Regardless of which approach is used, the estimated muscle forces remain sensitive to both the computational method used to resolve muscle force indeterminacy and the parameter values used in the neuromusculoskeletal model.

One way to address the dual problem of indeterminate muscle force solutions and unmeasurable model parameter values is to identify additional types of experimental data that could limit muscle force solutions and the model calibration process further. Neural control studies have shown that a large number of muscle EMG signals (8 to 32) collected during walking can be decomposed into three to six neural commands [35,73–75]. Recent work has also shown that neural commands extracted from a subset of experimentally measured EMG signals can reconstruct the shapes of the omitted EMG signals accurately [76]. Thus, it may be physiologically reasonable to use experimentally-derived neural commands as basis functions to construct *all* model-predicted muscle activations [50]. In addition, instrumented knee studies performed using force-measuring knee replacements have provided internal force data that permit at least two additional inverse dynamic knee loads to be used as constraints in the muscle force estimation and model calibration process [77,78]. While synergy-derived neural commands can limit only muscle activation shapes, knee contact force measurements can limit both the amplitudes *and* shapes of predicted activations.

This study investigates how knowledge of knee contact forces affects calibration of neuromusculoskeletal model parameter values and subsequent prediction of leg muscle and

knee contact forces. The two primary questions investigated were the following. First, can a static optimization that uses a well-calibrated neuromusculoskeletal model predict experimental knee contact forces accurately for multiple gait trials? This question addresses whether poorly calibrated model parameter values may be just as critical as an indeterminate muscle force solution in affecting predicted leg muscle and knee contact forces during walking. Second, which muscle-tendon model parameter values change the most when experimentally measured knee contact forces are not used as part of the model calibration process? This question addresses whether particular types of parameters or particular muscles require more refined calibration methods to achieve accurate knee contact force predictions. The static optimization approach used to address these questions limits predicted activations to be close to scaled experimental EMG signals (for muscles with experimental EMG data) or linear combinations of experimental neural commands (for muscles without experimental EMG data).

4.2. Methods

4.2.1 Experimental data

Experimental data for this study were obtained from the Fourth Grand Challenge Competition to Predict In Vivo Knee Loads [77]. Surface marker, ground reaction, electromyographic (EMG), knee contact force, and single-plane fluoroscopic knee motion data were available from a single subject (gender: male, age: 88 years, mass: 65 kg, height: 166 cm) implanted with a force-measuring tibial prosthesis (right knee). The prosthesis possessed four uniaxial load cells located in the four quadrants of the tibial tray [79]. Six normal overground gait trials performed at a self-selected speed (1.26 ± 0.03 m/s) were selected for analysis. Available data included trajectories of 53 surface markers, ground reactions from three force plates, knee contact forces from the instrumented implant, and EMG data from 10 muscles (Adductor Magnus - Addmag; Biceps Femoris Longhead - Bflh; Gastrocnemius Lateralis - GasLat; Gastrocnemius Medialis - GasMed; Peroneus Longus - PerLong; Semimembranosus - Semimem; Soleus - Sol; Tibialis Anterior - TibAnt; Tensor Fascia Latae - TFL; Vastus Lateralis - VasLat).

The experimental data were processed using standard methods. The EMG data were high-pass filtered (fourth-order zero phase-lag Butterworth at 30 Hz), full-wave rectified, demeaned, and low-pass filtered (fourth-order zero phase-lag Butterworth at 6 Hz). Each processed EMG signal was resampled to 101 data points and normalized to its maximum value over all movement trials from the Fourth Grand Challenge Competition, including trials from other walking conditions (e.g., medial thrust gait). Ground reaction and knee contact force data were also low-pass filtered in a consistent manner (fourth-order zero phase-lag Butterworth at 6 Hz [80].

4.2.2 Muscle synergy analysis

Experimental neural commands were calculated by performing muscle synergy analysis on the 10 processed muscle EMG signals after they were passed through an activation dynamics model. Activation dynamics was modeled using a first-order ordinary differential equation [81], where the activation and deactivation time constants for each muscle were taken from the literature [82]. Muscle synergy analysis was performed on the experimental activations using a non-negative matrix factorization algorithm [39,50,83]. The analysis decomposed the 10 experimental activations into a pre-defined number of synergies (< 10), where each synergy consisted of a single time-varying neural command with a corresponding set of time-invariant weights (called a "synergy vector") describing how the neural command contributed to each experimental activation. Each synergy vector was normalized to a maximum value of one, and its associated neural command was scaled such that the product of the synergy vector and its neural command did not change. The analysis was performed iteratively with the pre-defined number of synergies incremented by one each time until the total variance accounted surpassed 90%, which required 5 synergies.

4.2.3 Musculoskeletal model analyses

A subject-specific musculoskeletal model of the pelvis and right leg (femur, patella, tibia/fibula, and foot) of the subject [77] was constructed in OpenSim [84] and used to calculate joint kinematics and inverse dynamic loads for the six normal walking trials. The model incorporated subject-specific bone and implant geometry and possessed 17 degrees of freedom (DOFs): 3 translations and 3 rotations defining the position and orientation of the pelvis with respect to ground, 3 rotations (flexion, adduction, and rotation) for the hip joint,

3 rotations (flexion, adduction, and rotation) and 3 translations (superior-inferior, anterior-posterior, and medial-lateral) for the knee, and 2 rotations (flexion and eversion) for the ankle. A published OpenSim lower-body model possessing 44 muscle-tendon actuators on each leg [68] was scaled to match the subject-specific geometry, and muscle origins, insertions, and wrapping surfaces were transferred to the subject-specific model. The same published model was used to prescribe patellar motion with respect to the femur as a function of knee flexion angle. No ligaments were included in the model.

Knee kinematics (3 rotations and 3 translations) consistent with the knee contact force measurements from each gait trial were calculated in Matlab using an elastic foundation contact model of the subject's femoral component and tibial insert [85]. First, initial OpenSim inverse kinematic analyses were performed with all tibiofemoral DOFs except flexion locked to neutral values. These analyses provided an initial estimate of the knee flexion time history for each gait trial. Next, the pose of the femoral component on the tibial insert was estimated by performing a nonlinear least squares optimization for each time frame of each gait trial. The optimization locked three DOFs (flexion angle from inverse kinematics, internal-external rotation and anterior-posterior translation from fluoroscopy) and adjusted three DOFs (superior-inferior translation, medial-lateral translation, and varus-valgus rotation) to match the experimentally measured medial and lateral compressive contact forces and a medial-lateral shear contact force of zero.

OpenSim analyses were performed to calculate joint kinematics, inverse dynamic loads, muscle-tendon lengths and velocities, and muscle moment arms as required for the subsequent muscle force optimizations. For each gait trial, a second OpenSim inverse kinematic analysis was performed where all tibiofemoral DOFs except flexion were prescribed to match their values from the pose estimation optimizations. The resulting joint kinematics were filtered (four-order zero phase-lag Butterworth at 6 Hz) prior to performing an OpenSim inverse dynamic analysis that calculated net loads for three hip, six knee, and two ankle DOFs. The filtered joint kinematics were also used in an OpenSim muscle analysis that calculated muscle-tendon length and velocity and muscle moment arm time histories for all muscles in the model.

Muscle force generation was modeled in Matlab using a custom Hill-type model with a rigid tendon. The model possessed normalized force-length and force-velocity characteristics and included both active and passive force generation. Peak isometric strength values were taken to be twice literature values [86], while pennation angles were taken directly from the literature [68]. Initial values for optimal muscle fiber lengths and tendon slack lengths were taken as scaled literature values [68]. Muscle-tendon model inputs included activation, optimal muscle fiber length, and tendon slack length values guessed by the two-level optimization described below and muscle-tendon length and velocity information provided by the final OpenSim inverse kinematic analysis.

4.2.4 Optimization problem formulations

We formulated a two-level optimization problem in Matlab to calibrate neuromusculoskeletal model parameter values to data from the six selected gait trials. The outer-level optimization used a non-linear least squares algorithm to adjust design variables related to time-invariant model parameter values (optimal muscle fiber length scale factors, tendon slack length scale factors, muscle moment arm offsets, activation scale factors for muscles with experimental EMG data, and synergy vector weights for muscles without experimental EMG data), while the inner-level optimization used a fast quadratic programming algorithm applied to one time frame at a time of all six gait trials to adjust design variables for time-varying muscle activations given the current guess for model parameter values (Figure 4.1). The outer-level cost function minimized a weighted sum of squares of terms that included passive muscle forces, moment arm offsets, activation deviations away from synergy-based activation estimates (i.e., linear combinations of experimental neural commands), and reserve activations (strength 0.5 Nm) required to balance six inverse dynamic loads. Sixteen of the forty-four muscle bundles were associated with one of the ten experimental EMG signals (Table A.2, Appendix A). For those muscles with associated experimental EMG data, minimizing activation deviations away from synergy-based estimates is similar to tracking experimental activations directly. In addition, the outer-level cost function included penalty terms raised to a higher power that bounded optimal muscle fiber length and tendon slack length scale factors to remain within 20% of 1 while also remaining within 20% of each other, activation scale factors to remain between 0.1 and 1, synergy-based activation estimates to remain between 0 and 0.7, average values of

normalized muscle lengths for related muscles (Table A.3, Appendix A) to remain within 10% of each other, and moment arm offsets for related muscles (Table A.4, Appendix A) to remain within 5 mm (for moment loads) or 0.015 (for sup-inf force contributions) of each other. The inner-level cost function minimized the sum of squares of muscle and reserve activations [87] subject to equality constraints that six inverse dynamic loads (three hip, one knee only for flexion, and two ankle) be matched, and bound constraints that predicted activations be within ± 0.05 of synergy-based activation estimates and remain between a small positive value (to prevent a singularity in the Hill-type muscle model) and 1.

To explore how knowledge of knee contact forces affects model calibration and estimated leg muscle and knee contact forces, we formulated the outer-level cost function two ways. The first way (henceforth called "Approach A") introduced additional weighted terms that minimized the sum of squares of errors in medial and lateral knee contact forces. Experimental medial and lateral knee contact forces were calculated from the four load cell measurements using a validated regression relationship [77]. Model medial and lateral knee contact forces were calculated by subtracting muscle contributions to the superior-inferior force and varus-valgus moment from inverse dynamics and then converting the axial contact force and coronal contact moment into an equivalent medial and lateral force via an additional validated regression relationship [77]. Since no terms existed in the inner-level cost function to track medial and lateral knee contact forces, close matching of these quantities by the inner-level optimization could only occur through proper calibration of model parameter values by the outer-level optimization. The second way (henceforth called "Approach B") did not introduce these additional terms to the outer-level cost function and thus did not use any experimental contact force information during the model calibration process. Both approaches used an identical inner-level problem formulation.

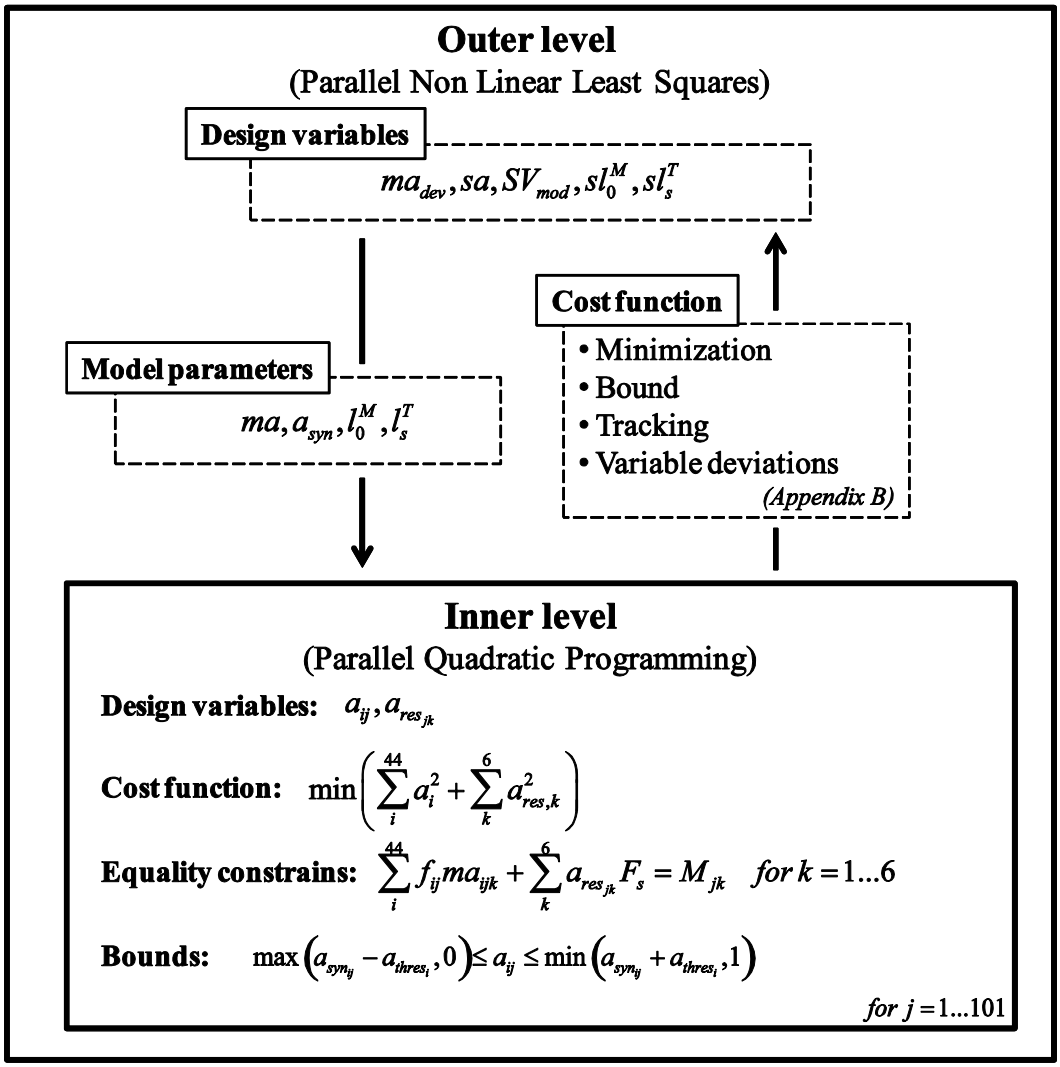

Figure 4.1. Block-diagram of the two-step optimization formulation. a_{syn} stands for reconstructed activations from synergy components, ma and ma_{dev} moment arm and moment arm deviation respectively, sa is the scale factor for experimental a_{syn}, SV_{mod} model synergy vector, l_0^M and sl_s^T optimal fiber length and its scale factor, l_s^T and sl_s^T slack length of the tendon and its scale factor, a muscle model activation, a_{res} reserve activation, F_s strength of the reserve actuators which is 0.5 Nm, a_{thres} the half of the allowed range of variation (0.01 for muscles with experimental EMG associated and 0.05 for the others), f muscle force and M the inverse dynamics moment. *i is the muscle (44 muscles), j* is the time frame (101 frames) and *k* is the tracked joint moment (6 loads).

4.2.5 Data analysis

We evaluated how knowledge of knee contact forces affected calibration of model parameter values and subsequent prediction of leg muscle and knee contact forces using several quantitative measures. Similarity of calibrated model parameter values between the two approaches was quantified by calculating percent or absolute change of Approach B values relative to Approach A values. Those changes were calculated for medial, central, lateral, and all leg muscles and evaluated statistically using two-tailed *t*-tests (see Table A.1 in

Appendix A for description of muscle groupings). Accuracy of knee contact force predictions for the two approaches relative to experimental measurements was quantified by calculating the coefficient of determination R^2 as a measure of magnitude and shape differences, root mean square error *RMSE* as a measure of magnitude differences, and the correlation coefficient *r* as a measure of shape differences. These measures from the two approaches were compared statistically for the six gait trials using two-tailed paired *t*-tests. Similarity of knee contact and leg muscle force predictions between the two approaches was quantified by calculating mean differences along with R^2, root mean square difference *RMSD*, and *r* values. Mean differences were evaluated statistically relative to zero for the six gait trials using two-tailed *t*-tests.

To seek to understand how model parameter value changes led to knee contact and leg muscle force changes, we also evaluated changes in normalized muscle lengths and muscle activations. Similarity of normalized muscle length predictions between the two approaches was quantified by calculating mean difference, R^2, *RMSD*, and *r* values, where mean differences were evaluated statistically. Accuracy of predicted activations relative to EMG-derived activations (muscles with EMG data) or relative to synergy-based activation estimates (muscles without EMG data) was assessed using R^2, *RMSE*, and *r* values, which were also compared statistically between the two approaches. Similarity of predicted activations between the two approaches was quantified by calculating mean difference, R^2 (when reasonable), *RMSD*, and *r* values with statistical evaluation of mean differences.

4.3. Results

4.3.1 Muscle parameters

Overall, optimal fiber lengths between Approaches were different (p=0.002). They were higher in Approach B by an average of 6 mm (8.5%). In particular, lateral muscles had the highest differences (Table 4.1). In Approach B, 30 of 44 muscles (medial, lateral and central) had optimal fiber lengths higher than in Approach A. Tendon slack lengths were not statistically different between the two approaches (p=0.27), though large differences existed for many muscles. In Approach B, 18 muscles (medial, lateral and central) had tendon slack lengths higher than in Approach A.

There were statistical differences in scale factors for experimental muscle activations between approaches (Table 4.1). Scale factors were higher in Approach B for medial muscles (p=0.01) whereas they were higher in Approach A for central muscles (p=0.05). Given that scale factors were limited to be between 0 and 1, the variability for lateral muscles was high (-0.07 ± 0.59).

Mean moment arms were similar between approaches for all muscle groups (medial, central and lateral) and exhibited no statistical differences (Table 4.1). However, variability between approaches was high (up to 14.1 mm for central muscles). Comparing the adjusted moment arms at each joint to the subject-specific OpenSim model, knee flexion moment arms were statistically higher for Approach A (14±9 mm, 33.8±18.4 %, p<0.001), see Table A.7 (Appendix A) and lower for Approach B (-1±5 mm, -5.5±19.7 %, p=0.04).

Table 4.1. Similarity of model parameter values obtained in Approach B relative to A, for central, lateral, and all muscles from 6 gait trials. Similarities are reported as percent differences for optimal fiber lengths l_o^M and slack length of the tendons l_s^T, and as absolute differences for scale factor of experimental muscle activations *sa* and moment arm deviations ma_{dev} (in mm). Statistically significant differences ($p < 0.05$) in mean values relative to zero are indicated by a star (*).

Quantity	Medial	Central	Lateral	All
l_o^M *(%)*	4.90±12.78	9.23±17.81	13.00±15.49*	8.54±14.76*
l_s^T *(%)*	1.41±11.00	-1.47±4.80	-0.86±11.59	0.13±10.39
sa	0.31±0.25*	-0.05±0.01*	-0.07±0.59	0.12±0.43
ma_{dev} (mm)	-1.9±10.1	-1.9±14.1	-0.7±9.3	-1.5±10.4

4.3.2 Knee contact forces

The shape and magnitude of knee contact forces were accurately predicted for Approach A (average R^2>0.88, average *RMSE*<93 N, average r>0.95) but not for Approach B (average R^2<0.1, average *RMSE*>323 N, average r<0.90) (see Table 4.2). For Approach B, medial contact force was over predicted but maintained a similar shape (Figure 4.2), while lateral contact force had peaks in the beginning of the stance and swing phase that were present in the experimental forces.

Medial, lateral and total contact force prediction accuracies were statistically different between approaches in terms of R^2, *RMSE*, and *r values* (p<0.001 for medial, lateral, and

total in all cases; see Table 4.2). Mean values of knee contact forces were also different between approaches ($p<0.001$ for medial, lateral, and total), see Table 4.3.

Table 4.2. Medial, lateral and total contact force accuracy for both approaches. Mean and standard deviations of R^2, *RMSE* and *r* values. Statistically significant differences ($p<0.05$) between the same quantities from both approaches are indicated by a star (*).

Quantity	Approach	Medial	Lateral	Total
R^2	A	0.97±0.01*	0.88±0.05*	0.96±0.02*
	B	0.10±0.28*	-3.43±1.74*	-0.36±0.24*
RMSE (N)	A	52.62±16.37*	56.63±9.54*	92.80±26.03*
	B	322.76±63.89*	347.79±33.09*	559.90±32.11*
r	A	0.99±0.01*	0.95±0.02*	0.98±0.01*
	B	0.90±0.03*	-0.10±0.10*	0.74±0.07*

Table 4.3. Medial, lateral and total contact force similarities. Mean and standard deviations of mean contact force difference, R^2, *RMSD* and *r* values between approaches. Statistically significant differences ($p<0.05$) between mean values from both approaches are indicated by a star (*).

Quantity	Medial	Lateral	Total
MeanD (N)	223.9±50.15*	143.8±38.8*	367.7±80.3*
R^2	0.15±0.22	-2.82±1.44	-0.23±0.19
RMSD (N)	315.15±60.25	330.51±25.68	530.47±30.67
r	0.91±0.02	0.05±0.04	0.79±0.09

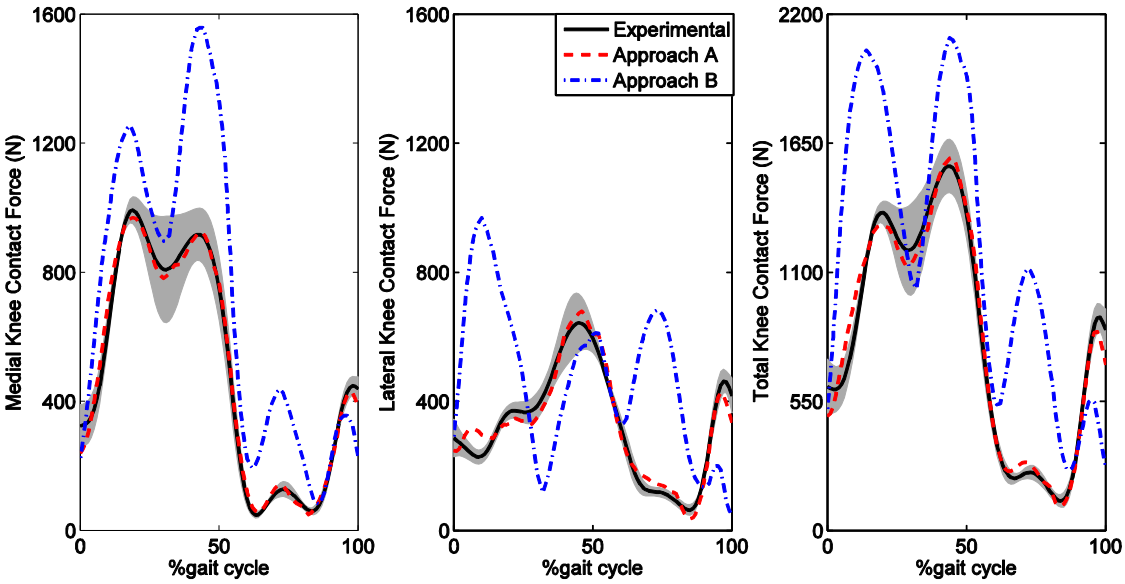

Figure 4.2. Experimental knee contact forces and mean knee contact force predictions for each approach (A and B). The grey area corresponds to the mean ±1 standard deviation for the experimental forces.

4.3.3 Leg muscle forces

Changes in calibrated muscle parameter values lead to differences in muscle force predictions. Most mean muscle forces were different between approaches (29 muscles with $p<0.05$). Overall they were higher in Approach B by 9.58 N. Lateral muscles had the greatest differences between approaches ($p<0.001$; see Table 4.4). Eight muscles had mean force differences between approaches that were larger than 40 N and five were lateral muscles (bflh, bfsh, glmed1, glmed3, and vaslat). Some muscle forces were higher in Approach B, while others were higher in Approach A (Figure 4.3).

Table 4.4. Similarity of model muscle forces obtained in Approach B relative to A, for medial, central, lateral, and all muscles from 6 gait trials. Mean and standard deviations of mean muscle forces, R^2, *RMSD* and *r* values between approaches. Statistically significant differences ($p<0.05$) between mean values from both approaches are indicated by a star (*).

Quantity	Medial	Central	Lateral	All
MeanD (N)	-3.13±7.46	13.91±7.05*	24.35±4.11*	9.58±2.66*
R^2	-4.61±2.00	-1.24±1.42	-90.70±13.73	-36.19±5.24
RMSD (N)	64.5±6.4	86.7±21.88	79.77±7.16	73.6±7.64
r	0.71±0.07	0.63±0.15	0.59±0.03	0.66±0.04

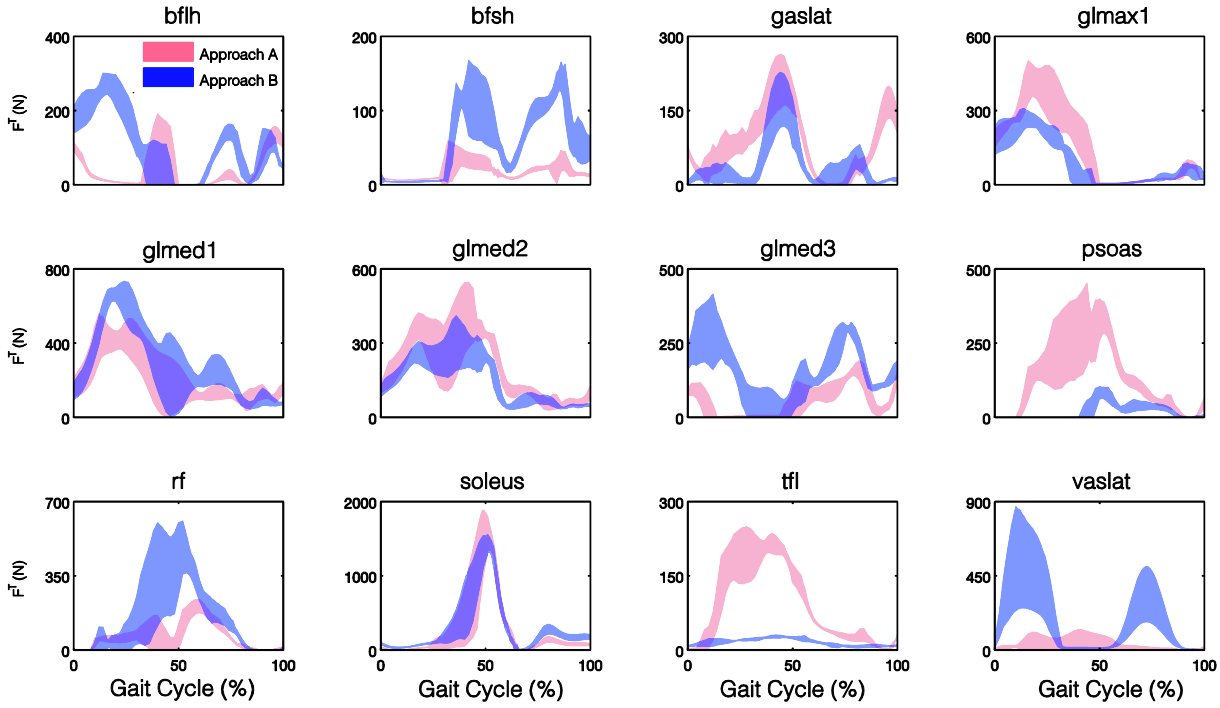

Figure 4.3. Muscle force values for muscles with the greatest mean differences between approaches A and B. The plotted area corresponds to the mean ± 1 standard deviation of all trials.

4.3.4 Other relevant quantities

Mean normalized fiber lengths were different for all muscles, though the shapes of the normalized fiber length curves were nearly identical between the two approaches (Table 4.5). In absolute terms, mean differences between approaches were small, and all curves remained within physiological operating ranges (Figure 4.4) [88,89]. Observed variations were consistent with the differences in passive muscle forces between the two approaches (Table 4.6), which were statistically different for 43 muscles (p<0.05). Passive forces were lower than 40 N for most muscles in both approaches.

Table 4.5. Similarity of model normalized fiber lengths obtained in Approach B relative to A, for medial, central, lateral, and all muscles from 6 gait trials. Mean and standard deviations of mean normalized fiber forces, R^2, *RMSD* and *r* values between approaches. Statistically significant differences (p<0.05) between mean values from both approaches are indicated by a star (*).

Quantity	Medial	Central	Lateral	All
MeanD	-0.031±0.000*	-0.047±0.000*	-0.063±0.003*	-0.045±0.001*
R^2	-3.66±0.93	-6.65±0.94	-5.62±1.06	-4.85±0.47
RMSD	0.075±0.000	0.125±0.000	0.128±0.003	0.102±0.001
r	1±0.00	1±0.00	1±0.00	1±0.00

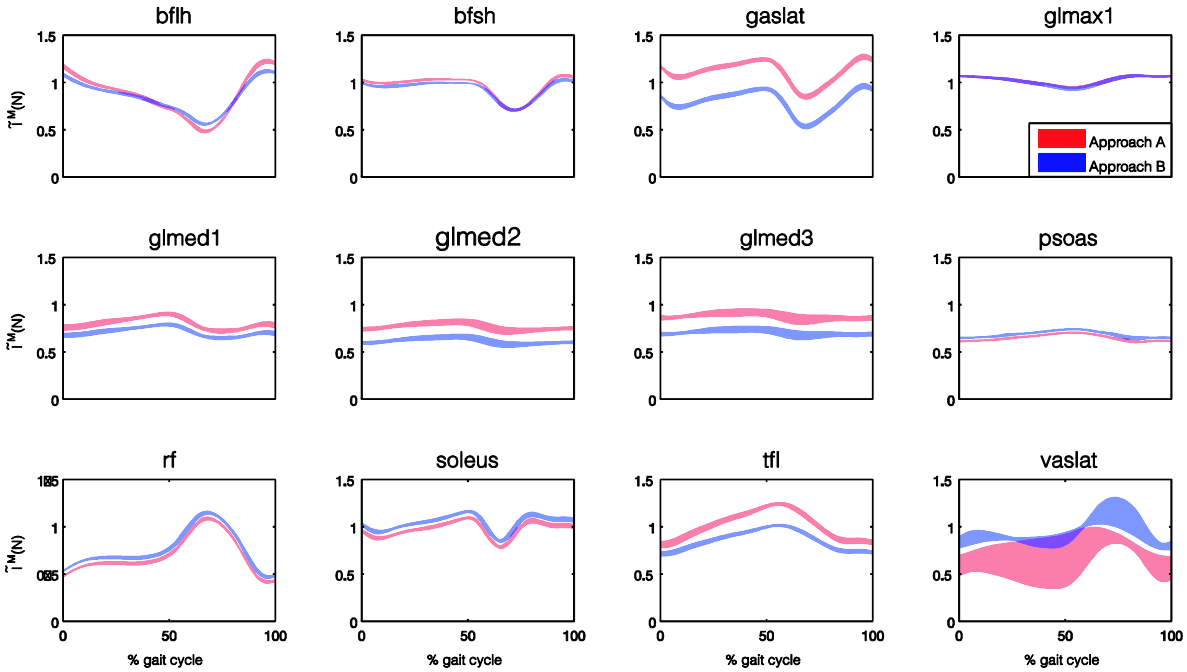

Figure 4.4. Normalized fiber lengths for muscles with the greatest differences in mean tendon forces between approaches A and B. The plotted area corresponds to the mean ± 1 standard deviation of all trials.

Table 4.6. Similarity of model passive forces obtained in Approach B relative to A, for medial, central, lateral, and all muscles from 6 gait trials. Mean and standard deviations of mean passive forces, R^2, *RMSD* and *r* values between approaches. Statistically significant differences (p<0.05) between mean values from both approaches are indicated by a star (*).

Quantity	Medial	Central	Lateral	All
MeanD	-4.30±0.61*	1.50±1.57	0.17±1.15	-1.75±0.86*
R^2	-4.69±1.16	-4.87±0.44	-636.43±152.44	-234.44±55.03
RMSD	12.24±0.81	33.83±1.43	23.83±2.09	19.89±1.06
r	0.91±0.00	1.00±0.00	0.93±0.09	0.93±0.03

Predicted muscle activations demonstrated different trends between the two approaches. For tracking of experimental and synergy-based activations, muscles with experimental EMG data had the lowest magnitude errors (lower mean *RMSE* values for Approach A) but highest shape errors (lower mean *r* values for Approach A) (see Tables 4.7 and 4.8). *RMS errors* were statistically different between the approaches (p<0.05) for all groups (medial, central and lateral muscles) and were generally lower for Approach B, while *r* values were statistically different between approaches for lateral muscles with associated experimental EMG (p=0.01, Figure 4.5) and medial muscles without associated experimental EMG data (p=0.004). Comparing predicted activations from the two approaches (Table 4.9), activation shapes were most similar for medial muscles (r=0.70) and least similar for lateral muscles (r=0.52). Mean activations were similar for both approaches, with any statistically significant differences and of limited practical importance. Nonetheless, *RMS* differences between approaches were on the order of 0.1 for all groups.

Table 4.7. Accuracy of muscle activation predictions for the 16 muscles with associated experimental EMG data relative to their activations reconstructed from synergy components. Values indicate mean ± standard deviation from 6 gait trials. Statistically significant differences (p < 0.05) between the same quantities from both approaches are indicated by a star (*).

Quantity	Approach	Medial	Central	Lateral	All
R^2	A	-1.51±0.35*	-0.20±0.31	-0.85±0.27*	-1.10±0.24*
	B	-0.96±0.35*	-0.24±0.20	-0.18±0.13*	-0.58±0.24*
RMSE	A	0.05±0.00*	0.14±0.02*	0.11±0.01*	0.09±0.00*
	B	0.08±0.01*	0.12±0.01*	0.07±0.01*	0.08±0.00*
r	A	0.37±0.14	0.55±0.19	0.28±0.13*	0.36±0.11*
	B	0.43±0.18	0.57±0.14	0.44±0.04*	0.45±0.11*

Table 4.8. Accuracy of muscle activation predictions for the 28 muscles without associated experimental EMG data relative to their activations reconstructed from synergy components. Values indicate mean ± standard deviation from 6 gait trials. Statistically significant differences ($p < 0.05$) between the same quantities from both approaches are indicated by a star (*).

Quantity	Approach	Medial	Central	Lateral	All
R^2	A	-0.15±0.26*	-0.10±0.41	0.29±0.20	0.01±0.20*
	B	0.08±0.21*	0.32±0.22	0.17±0.05	0.15±0.11*
RMSE	A	0.17±0.02*	0.13±0.03*	0.07±0.01*	0.13±0.02*
	B	0.12±0.02*	0.08±0.02*	0.10±0.01*	0.11±0.01*
r	A	0.42±0.14*	0.47±0.31	0.64±0.14	0.51±0.12*
	B	0.57±0.13*	0.71±0.13	0.56±0.03	0.59±0.07*

Table 4.9. Similarity of muscle activation predictions in Approach B relative to A, for medial, central, lateral, and all muscles from 6 gait trials. Values indicate mean ± standard deviation from 6 gait trials. Mean and standard deviations of mean model activations, R^2, *RMSD* and *r* values between approaches. Statistically significant differences ($p<0.05$) between mean values from both approaches are indicated by a star (*).

Quantity	Medial	Central	Lateral	All
MeanD	-0.000±0.007	0.004±0.011	0.021±0.005*	0.009±0.004*
R^2	—	-1.46±1.30	-47.75±15.57	—
RMSD	0.08±0.01	0.09±0.02	0.09±0.01	0.09±0.01
r	0.70±0.07	0.67±0.14	0.52±0.03	0.63±0.05

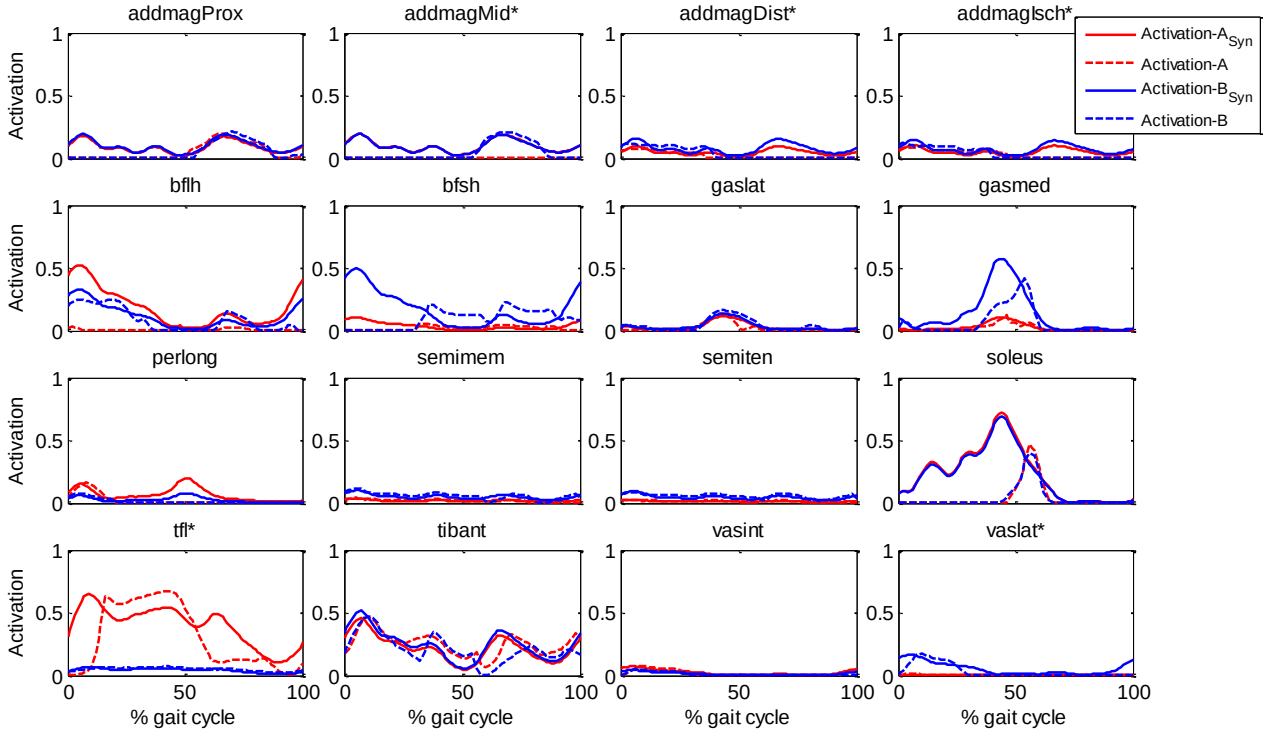

Figure 4.5. Activations reconstructed from synergy components (a_{Syn}, in solid lines) and model activations (Activations, in dashed lines) for muscles with associated experimental EMG. Asterisk* stands for statistically different *r* values between approaches A and B.

4.4. Discussion

The goal of this study was to investigate differences in knee contact and leg muscle force predictions when those forces were used to calibrate the model (Approach A) and when no contact forces were available (Approach B), which is the most usual case. The algorithm to predict those forces consisted of a two-step synergy-based algorithm, which calibrated muscle parameters and predicted knee muscle and contact forces considering that muscle synergies helped to predict knee contact forces [50]. The most significant result was that one set of muscle-tendon parameters allowed static optimization to predict both medial and lateral knee contact forces with high accuracy in terms of magnitude (average *RMSE*=52.6N medial and *RMSE*=56.6 lateral) and shape (average *r*=0.99 medial and *r*=0.95 lateral). This accuracy was similar or higher than the obtained in other studies that predicted unblinded knee contact forces for one gait trial [50,90]. As expected, when knee contact forces were not used during the calibration process, their prediction was poorer. Medial contact force was overpredicted (average *RMSE*=322.8N and *r*=0.90) and lateral contact force had a significantly different shape compared to the experimental one (*RMSE*=347.8N and *r*=-0.1). These results indicated that the use of muscle synergies was not sufficient to obtain a good contact force prediction when no contact force information was used to calibrate the model.

The differences in the calibration of muscle parameter values between approaches A and B can explain the variations in muscle and knee contact force predictions. The use of knee contact force information when calibrating muscle parameters (Approach A) led to different muscle moment arms, especially in knee flexion and hip rotation moments, which were higher than in Approach B. Moreover, optimal fiber lengths for lateral muscles were statistically higher when no contact forces were used during the calibration. Scale factors of muscle activations for muscles with associated EMG also had differences between approaches. This fact suggests that a better calibration of model parameter values was achieved in Approach A and, therefore, those differences in model parameters between approaches led to different normalized fiber lengths, and thus different activations and muscle forces.

It was observed that the main differences between both analyzed approaches came from muscle activations and forces of the lateral muscles. From the eight muscles with greatest

differences in tendon forces (>40N), five of them were from the lateral side (bflh, bfsh, glmed1, glmed3, and vaslat). It is possible that the use of alternate motion patterns (especially ones that preferentially excite lateral muscles) in the calibration process could improve the similarity of calibrated muscle-tendon model parameter values. Our hypothesis was that those muscles would have a higher contribution to hip adduction and subtalar moments (tracked in the inner level) and a better calibration could be achieved.

Overfitting is a common issue in optimization problems. In our study, muscle activations were predicted in an inner level for six gait trials at a time, where muscle parameters could not be changed and no knee contact force information was transferred from the outer to the inner level. Therefore, there was no guarantee that another set of muscle parameters made the prediction of knee contact forces as accurate as the obtained one. Nevertheless, we tried the same algorithm (same cost functions and optimization formulations) to calibrate muscle parameters with three overground gait trials (outer and inner level) and then, we predicted knee contact forces with other three overground gait trials (only inner level) with the previously obtained muscle parameters. The results suggested that the obtained set of muscle parameters could predict the knee contact forces with high accuracy (Appendix A.3, Figure A.1). Further validations of the presented formulation are out of the scope of this study. In order to validate the formulation in different motions, other trials should be used when calibrating and predicting. The formulation should also be validated in other subjects wearing a knee instrumented implant. Muscle parameter calibration is critical as suggested by other studies. For example, Manal and Buchanan [91] reported knee contact force predictions for two trials (normal walking and medial thrust gait). However, to obtain accurate knee contact force predictions for both trials, they had to make some model parameter values different from the two trials. In contrast, in the presented study one set of muscle parameters was obtained that predicted accurately knee contact forces for six trials at a time (Approach A).

This study had several limitations. They were based on the number of tested subjects and the number of different experimental trials. Data for only one subject was used to calculate knee muscle and contact forces, further analysis in other subjects should be carried out to validate the formulation in other individuals. As suggested, the use of other type of trials in which

lateral muscles play a more important role could improve the calibration of these muscle parameters. As future work, the formulation will be tested in other human movements, such as in crouch gait, trunk sway or doing squats in one leg. The lateral ligaments would be more stressed in those trials [92], so, a proper ligament model should be used to reproduce the physiological joint dynamics. Other future work could be focused on investigating whether adding more physiological constrains, when no knee contact force information is used during the calibration, could allow obtaining better knee contact force predictions. On the one hand, less neural commands would decrease the indeterminacy of the muscle activation calculation. And, on the other hand, proper moment arm relations could be used to modify the muscle contributions to the knee superior-inferior force or the muscle adduction moment when no contact forces are available.

In conclusion, one set of muscle-tendon parameters that predicts knee contact forces with high accuracy was obtained calibrating six gait trials at a time. It was demonstrated that when no knee contact force information was available, poorer knee contact forces were obtained, especially for the lateral knee contact force. In order to obtain a higher accuracy of the knee contact force predictions when those forces are not available, future work should be focused on calibrating the model with trials which lead to a better calibration of lateral muscles.

Chapter 5

Conclusions

This thesis comprises three works related to the study of muscle actuation redundancy during walking. In the first one, a simple static optimization approach to predict muscle forces in a single ACL-deficient subject is introduced; secondly, the differences in muscle excitation patterns of ACL-deficient and healthy subjects are investigated through a muscle synergy analysis; and finally, in the last study, a patient-specific model to predict physiologically consistent muscle and knee contact forces is presented.

The first study was aimed at analyzing what cost function best fitted model muscle activations and EMG signals in a subject with ACL-deficiency. A generic musculoskeletal model with 8 muscles was scaled in OpenSim to apply inverse kinematics and inverse dynamics. The resultant inverse dynamics loads were consistent with other studies related to ACL-deficient subjects. The results showed that a weighted cost function penalizing biarticular muscles acting on the hip and the knee (Hamstrings and Rectus Femoris) best fitted muscle activations and EMG signals. The hypothesis was fulfilled, since the obtained best cost function lead to different magnitudes of model muscle activations compared to an equally weighted cost function. Some limitations need to be noticed, for example the fact that static optimization itself (only minimizing a cost function) avoids co-contraction of antagonistic muscles. Furthermore, in order to get stronger conclusions, such study should be carried out with more subjects, as well as with different ways to group the muscles in the cost function.

With these limitations in mind, the second study was carried out to compare muscle excitations in a group of ACL-deficient subjects and a group of healthy subjects. ACL-deficient subjects were selected by clinicians of the Knee Surgery Unit at the Catalan Institute of Trauma and Sport Medicine (ICATME). Muscle excitations were studied at two levels: EMG signals (onset-offset patterns) and muscle synergies. As far as the author is concerned, no previous muscle synergy analysis in a group of ACL-deficient subjects appears in the literature thus far. EMG data of 8 muscles per leg were measured in 10 healthy subjects and 18 ACL-deficient subjects (before the surgery) when walking.

At the level of the onset-offset activation patterns, similar results to the literature were obtained since co-contraction between Quadriceps and Hamstrings in ACL-deficient subjects was longer than in healthy subjects. This fact suggested that these muscles actuated to stabilize the knee joint, that is, they co-contracted to prevent high displacements between the tibia and the femur.

At the level of muscle synergies, some differences were observed, like the higher peak in the fifth NC (which mainly activates Extensor Digitorum Longus) for the ipsilateral leg compared to the contralateral leg at the transition between the stance and the swing phases. The major use of ankle muscles in the ipsilateral leg as compared to the contralateral leg was in agreement with the fact that the control of the ipsilateral leg is shifted away from the injury, that is, from the knee to the ankle. Some differences between the Control group and injured subjects (both for ipsilateral and contralateral legs) were also identified: firstly, lower values in the first NC (mainly Gluteus Medius) in the Control group at early stance; secondly, lower values of the third NC (mainly Tibialis Anterior) in the Control group at middle stance; and finally, a greater peak of the second NC (mainly Gastrocnemius Lateralis and Soleus) in the Control group during the stance.

This study has the following limitations. In terms of mathematical decomposition of signals, more than one gait trial should be considered in a future work when calculating muscle SVs. In this case, the results would be more accurate. This aspect could not be accomplished due to space limitations of the laboratory. This study was carried out in ACL-deficient subjects before the surgical reconstruction. A future suggested study would be to involve

measurements after the surgery to observe how muscle synergies change in time after the reconstruction. With this knowledge, the surgeon and physiotherapist could have objective data to follow up the recovery of their patients.

In the third study, muscle synergies and optimization methods were combined to calculate physiologically consistent muscle and knee contact forces in six overground gait trials at a time. A two-step synergy-based optimization algorithm was developed to calibrate muscle parameters and calculate muscle activations. A patient-specific OpenSim model and fluoroscopy data allowed obtaining accurate kinematics of the leg and muscle-tendon lengths. In this case, *in vivo* knee contact forces were available, which gave the opportunity to validate model predictions.

When using knee contact forces to calibrate muscle parameters, the predictions of those forces were accurate in all six gait trials, while muscle parameters were within physiological ranges. In this case, obtained muscle activations were close to the ones generated from synergy components. Thus, it could be considered that muscle forces were physiological. When no *in vivo* contact forces were used during the calibration process, another set of calibrated muscle parameters was obtained, which led to different values of muscle activations and, therefore, also different values of model contact forces. In this approach, the accuracy of those forces compared to the experimental ones was poorer.

Analyzing what differences were the main responsible for changes in knee contact force predictions, it was observed that lateral muscle forces suffered major changes compared to the ones of central and medial muscles. This fact suggested that during the calibration process, other trials, including motions where lateral muscles had a more important role, should be considered. In such a case, the calibration for those muscles parameters would be more accurate, what would lead to better contact force predictions.

Further work should be done to make this algorithm useable for other subjects. The next steps would be the following: testing the formulation for other trials of the same subject (other gait velocities and other type of tasks), testing it in other subjects with instrumented prosthesis and, finally, using a formulation in real time for predicting muscle and knee contact forces in subjects who have no instrumented knee implants.

Appendix A

Supplementary data for the two-step optimization algorithm

A.1. Muscle classification

In the study presented in Chapter 4, muscles were grouped according their position showed in Table A.1.

Table A.1. Muscle groups according to their position.

Medial	Lateral	Central
adductor brevis	biceps femoris long head	extensor digitorus longus
adductor longus	biceps femoris short head	extensor hallucis longus
adductor magnus distal	gastrocnemius lateralis	flexor digitorum longus
adductor magnus middle	gemeli	flexor hallucis longus
adductor magnus ischial	gluteus medius anterior	rectus femoris
adductor magnus proximal	gluteus medius middle	soleus
gastrocnemius medialis	gluteus medius posterior	vastus interior
gluteus maximus superior	gluteus minimus anterior	
gluteus maximus middle	gluteus minimus middle	
gluteus maximus inferior	gluteus minimus posterior	
gracilis	peroneus brevis	
iliacus	peroneus longus	
pectineus	peroneus tertius	
psoas	periformis	
quadratus femoris	tensor fascia latae	
sartorius	vastus lateralis	
semimembranosus		
semitendinosus		
tibialis anterior		
tibialis posterior		
vastus medialis		

Some muscles were separated into bundles in our model, such as the adductor magnus (distal, ischial, middle and proximal and bundles) and only one EMG signal for adductor magnus was available. All bundles of those muscles were associated to have the same experimental synergy vector. Other muscles with no available EMG were close to others which exerted the same function and EMG was available, such as semitendinosus (close to semimembranosus). Those muscles were also considered to have the same experimental synergy vector (Table A.2).

Table A.2. Model muscles which are tracked with their corresponding experimental activity.

Experimental activation	Model muscles
adductor magnus	adductor magnus distal, adductor magnus ischial, adductor magnus middle, adductor magnus proximal
biceps femoris	biceps femoris long head, biceps femoris short head
gastrocnemius lateralis	gastrocnemius lateralis
gastrocnemius medialis	gastrocnemius medialis
peroneus longus	peroneus longus
semimembranosus	semimembranosus, semitendinosus
soleus	Soleus
tibialis anterior	tibialis anterior
tensor fascia latae	tensor fascia latae
vastus lateralis	vastus intermedius, vastus lateralis

A.2. Cost function formulation in the outer level

In the study presented in Chapter 4, muscle parameters were calibrated in the outer level of the two-step optimization. An algorithm to solve non-linear least squares problems (*lsqnonlin*) was used to get the optimal solutions. At this level, the cost function had four sets of terms aiming at:

- Minimizing variables (passive forces and residual reserve activations).
- Tracking variables (contact forces – only in Approach A – and muscle activations).
- Constraining variables into bounds (muscle moment arms, scale factors for activations from muscles with available EMG, reconstructed activations from synergies, and scale factors for optimal fiber lengths and slack lengths of the tendon).
- Allowing a uniform variation of normalized fiber lengths and muscle moment arms.

Detailed formulation of these terms is provided below. The number of the cost function terms is in parenthesis.

- **Minimization terms**

$$J_{F_{pe}^m} = \sum_{j}^{101}\sum_{i}^{44} 10\left(\frac{F_{pe_{ij}}^m}{F_{0_i}^m}\right)^2 \qquad (6x101x44) \tag{A.1}$$

where $F_{pe_{ij}}^m$ is the passive force of muscle *i* at time frame *j* and $F_{0_i}^m$ is the maximum isometric force of muscle *i*. It minimizes normalized muscle passive forces.

$$J_{res} = \sum_{j}^{101}\sum_{t}^{6} a_{res_{ij}}^2 \qquad (6x101x6) \tag{A.2}$$

where $a_{res_{ij}}$ is the reserve activation of muscle *i* at time frame *j*. It minimizes reserve activations.

- **Tracking terms**

$$J_{F_{med}} = \sum_{j}^{101}\left(\frac{\left(F_{med-\mathrm{mod}_j} - F_{med-exp_j}\right)}{20}\right)^2 \qquad (6x101\mathrm{or}\,0) \tag{A.3}$$

$$J_{F_{lat}} = \sum_{j}^{101}\left(\frac{\left(F_{lat-\mathrm{mod}_j} - F_{lat-exp_j}\right)}{20}\right)^2 \qquad (6x101\mathrm{or}\,0) \tag{A.4}$$

where $F_{med-mod_j}$ and $F_{med-exp_j}$ are the model and experimental knee medial contact forces respectively, *and* $F_{lat-mod_j}$ and $F_{lat-exp_j}$ are the model and experimental knee lateral contact forces respectively, at time frame *j*. These terms only appear when knee contact forces are used during the calibration (Approach A). They track medial and lateral knee contact forces, respectively.

$$J_a = \sum_{j}^{101}\sum_{i}^{44}\left(\frac{a_{mod\,ij} - a_{syn_{ij}}}{a_{thres}}\right)^2 \qquad (6x101x44) \tag{A.5}$$

where $a_{mod\,ij}$ and $a_{syn_{ij}}$ are the model activations and activations reconstructed from synergy components of muscle *i* at time frame *j*. a_{thres} is the half of the desired range of variation of model activation with respect to the activation reconstructed from EMG, it equals 0.05 for

muscles with associated experimental EMG and 0.01 for muscles without available EMG. It tracks activations reconstructed from synergy components.

- **Bound terms**

$$J_{ma} = 10 \sum_{k}^{n_{loads}} \sum_{i}^{n_{ma}} \left(\frac{ma_{dev_{ik}}}{ma_{thres_k}} \right)^2 \qquad (147 \text{ or } 121) \tag{A.6}$$

where ma_{dev} is the model moment arm deviation of muscle *i* at inverse dynamics load *k*. ma_{thres_k} is the half of the desired range of variation of moment arm deviation, it equals 5 mm for moment loads and 0.015 for the knee superior-inferior force. n_{loads} is the number of loads tracked by the two-step algorithm: 8 in Approach A (hip adduction, flexion and rotation moments, knee flexion and adduction moments, knee superior-inferior force, subtalar moment and ankle moment) and 6 in Approach B (the same as in A except knee adduction moment and sup-inf force). n_{ma} is the number of muscles with non-zero model muscle moment arm at joint *k*. It penalizes moment arm offsets higher than ma_{thres_k} .

$$J_p = 100 \sum_{s}^{16} \left(\frac{sa - 0.55}{0.45} \right)^{10} \qquad (16) \tag{A.7}$$

where sa is the scale factor for activation of muscle *s* with associated EMG. It constrains the scale factor for muscles with associated experimental EMG to be between 0.1 and 1.

$$J_{a_{syn}} = \sum_{j}^{101} \sum_{i}^{44} \left(\frac{a_{syn_{ij}} - 0.35}{0.35} \right)^{10} \qquad (6x101x44) \tag{A.8}$$

It constrains activations reconstructed from synergies to be between 0 and 0.7.

$$J_{sl_0^M} = \sum_{i}^{44} \left(\frac{sl_{0_i}^M - 1}{0.2} \right)^{10} \qquad (44) \tag{A.9}$$

where $sl_{0_i}^M$ is the scale factor for the optimal fiber length of muscle *i*. It constrains scale factors for optimal fiber lengths to be between 0.8 and 1.2.

$$J_{sl_s^T} = \sum_{i}^{44} \left(\frac{sl_{s_i}^T - 1}{0.2} \right)^{10} \qquad (44) \tag{A.10}$$

where $sl_{s_i}^T$ is the scale factor for the slack length of the tendon of muscle *i*. It constrains scale factors for slack length of the tendons to be between 0.8 and 1.2.

- **Variable deviation constrain terms**

$$J_{sl_0^M sl_s^T} = \sum_i^{44} \left(\frac{1}{0.2} \frac{sl_{0_i}^M - sl_{s_i}^T}{0.5\left(sl_{0_i}^M + sl_{s_i}^T\right)} \right)^{10} \qquad (44) \tag{A.11}$$

It penalizes deviations between scale factors of the slack length of tendons and the optimal fiber lengths higher than 20%.

$$J_{\tilde{l}^M dev} = \sum_u^{ngroups_{\tilde{l}^M}} \sum_v \left(\frac{\overline{\tilde{l}_u^M} - \overline{\tilde{l}_v^M}}{0.1} \right)^{10} \qquad (6x22) \tag{A.12}$$

It penalizes deviations of mean normalized fiber lengths higher than 0.1 for the pairs of muscles showed in Table A.3.

$$J_{maGroupdev} = \sum_u^{ngroups_{ma}} \sum_v \left(\frac{\overline{ma_u} - \overline{ma_v}}{ma_{thres}} \right)^{10} \qquad (6x30 \text{ or } 6x23) \tag{A.13}$$

It penalizes deviation of mean moment arms higher than 5 mm in moment loads, or 0.015 in the knee superior-inferior force contribution, for the pairs of muscles showed in Table A.4.

Table A.3. Groups of muscles with similar normalized fiber length. The first muscle of the group was the reference.

adductor magnus proximal, adductor magnus middle, adductor magnus distal, adductor magnus ischial
biceps femoris long head, biceps femoris short head
extensor digitorum longus, extensor hallucis longus
flexor digitorum longus, flexor hallucis longus
gastrocnemius lateralis, gastrocnemius medialis
gluteus maximus superior, gluteus maximus middle, gluteus maximus inferior
gluteus medius superior, gluteus medius middle, gluteus medius inferior
gluteus minimus superior, gluteus minimus middle, gluteus minimuz inferior
semimembranosus, semitendinosus, biceps femoris long head, gracilis
iliacus, psoas
peroneus brevis, peroneus longus
vastus intermedius, vastus medialis, vastus lateralis, rectus femoris
soleus, tibialis posterior

Table A.4. Groups of muscles with similar moment arm deviations. The first muscle of the group was the reference.

Hip flexion	biceps femoris long head, semimembranosus, semitendinosus
	gluteus minimus anterior, gluteus minimus middle
	gluteus medius anterior, gluteus medius middle, gluteus medius superior
Hip adduction	gluteus medius anterior, gluteus medius middle
	adductor magnus distal, adductor magnus ischial
	gluteus minimus anterior, gluteus minimus middle, gluteus minimus superior
	biceps femoris long head, semimembranosus
Hip rotation	adductor magnus proximal, adductor magnus middle, adductor magnus ischial
	semimembranosus, semitenendinosus
	gluteus maximus superior, gluteus maximus middle
Knee flexion	gracilis, semimembranosus
	vastus interior, vastus lateralis, vastus medialis
Knee adduction	semimembranosus, semitendinosus
	rectus femoris, vastus intermedius
Knee superior-inferior	biceps femoris long head, semimembranosus, semitendinosus
	vastus intermedius, vastus medialis, rectus femoris, Sartorius
Ankle	flexor digitorus longus, flexor hallucis longus
	gastrocnemius lateralis, gastrocnemius medialis
	peroneus brevis, peroneus longus
Subtalar	gastrocnemius lateralis, gastrocnemius medialis
	flexor digitorus longus, flexor hallucis longus, tibialis posterior

A.3. Supplementary results

Muscle parameters: optimal fiber lengths and slack lengths of the tendons. Tables A.5 and A.6 report mean and standard deviation of percent differences between model optimal fiber lengths and slack length of the tendon and literature values. Table A.7 shows the moment arm deviations for both approaches. Table A.8 shows the differences in moment arm deviations between both approaches.

Table A.5. Mean and standard deviation of percent difference of optimal fiber lengths from literature values.

Approach	Medial	Lateral	Central
A	6.5 ± 16.1	1.0 ± 16.9	8.2 ± 17.9
B	10.7 ± 13.8	12.8 ± 15.4	15.9 ± 10.0

Table A.6. Mean and standard deviation of percent difference of slack length of the tendons from literature values.

Approach	Medial	Lateral	Central
A	3.4 ± 16.3	5.8 ± 14.3	7.6 ± 5.6
B	4.2 ± 15.5	4.6 ± 16.3	5.9 ± 5.5

Table A.7. Mean and standard deviation of moment arm deviations for both approaches (in mm, except for sup-inf force which is dimensionless). In parenthesis, differences in percentage relative to mean moment arm. Asterisk* means statistically different from zero (p<0.05).

	A	B
Hip flexion	-2 ± 9 (43.7 ± 134.2)	-1 ± 12 (64 ± 179.4)
Hip adduction	0.08 ± 9 (22.8 ± 78.9)	0.03 ± 11 (40.9 ± 152.1)
Hip rotation	3 ± 8 (144.7 ± 421.1)	-2 ± 9 (6.1 ± 74.9)
Knee flexion	14 ± 9* (33.8 ± 18.4*)	-1 ± 5 (-5.5 ± 19.7)
Knee adduction	-1 ± 11 (20.5 ± 112.7)	NA
Knee sup-inf force	-0.004 ±0.011 (-0.4 ± 1.18)	NA
Ankle	1 ± 10 (10.9 ± 52.3)	4 ± 10 (16.2 ± 39.6)
Subtalar	-6 ± 11 (-16.1 ± 59.0)	0.07 ± 8 (90.0 ± 238.7)

Table A.8. Mean and standard deviation of absolute differences, and percentage differences between parenthesis, of moment arm deviations between approaches.

Quantity	Medial	Central	Lateral	All
$ma_{dev}\ hip_{flex}$	-0.3±11.7 (2.69±55.11)	0.3±0.9 (6.76)†	1.8±3.8 (18.56±26.82)	0.9±0.01 (8.72±45.40)
$ma_{dev}\ hip_{add}$	0.3±7.0 (32.35±104.73)	2.4±6.3 (95.44)†	-1.2±5.5 (5.53±38.39)	0.1±8.0 (25.03±85.73)
$ma_{dev}\ hip_{rot}$	-3.0±6.7 (4.04±139.33)	-0.7±1.7 (-31.66)†	-2.3±7.3 (-12.36±61.10)	-4.0±7.9* (-3.54±111.53)
$ma_{dev}\ knee_{flex}$	-3.0±6.6* (-20.16±13.99)*	-8.3±14.3 (-41.13±5.83)	-3.3±7.3 (-23.71±12.22)	-14.2±10.7* (-24.84±13.91)*
$ma_{dev}\ knee_{add}$	1.6±6.0 (174.22±269.74)	-2.5±4.3 (-66.10±16.29)	0.1±5.6 (22.77±76.27)	1.3±10.6 (78.95±204.02)
$ma_{dev}\ knee_{sup\text{-}inf}$	0.002±0.007 (0.64±1.34)	0.005±0.008 (1.75±0.27)	-0.001±0.003 (-0.37±0.54)	0.004±0.011 (0.42±1.20)
$ma_{dev}\ ankle$	0.1±4.6 (4.77±45.56)	0.8±8.2 (0.09±27.95)	1.5±3.4 (104.37±141.49)	2.7±9.7 (29.81±83.84)
$ma_{dev}\ subtalar$	0.1±0.5 (12.12±5.95)	1.2±8.3 (47.97±96.99)	1.5±6.5 (177.60±320.19)	3.4±10.2 (79.69±178.15)

†Only one value

A previous study, not presented in this document, was carried out in order to evaluate the ability to predict knee contact forces with gait trials which were not used during the calibration. In this case, three gait trials were used to calibrate muscle parameters and other three gait trials were used to predict knee contact forces. The results are shown in Figure A.1.

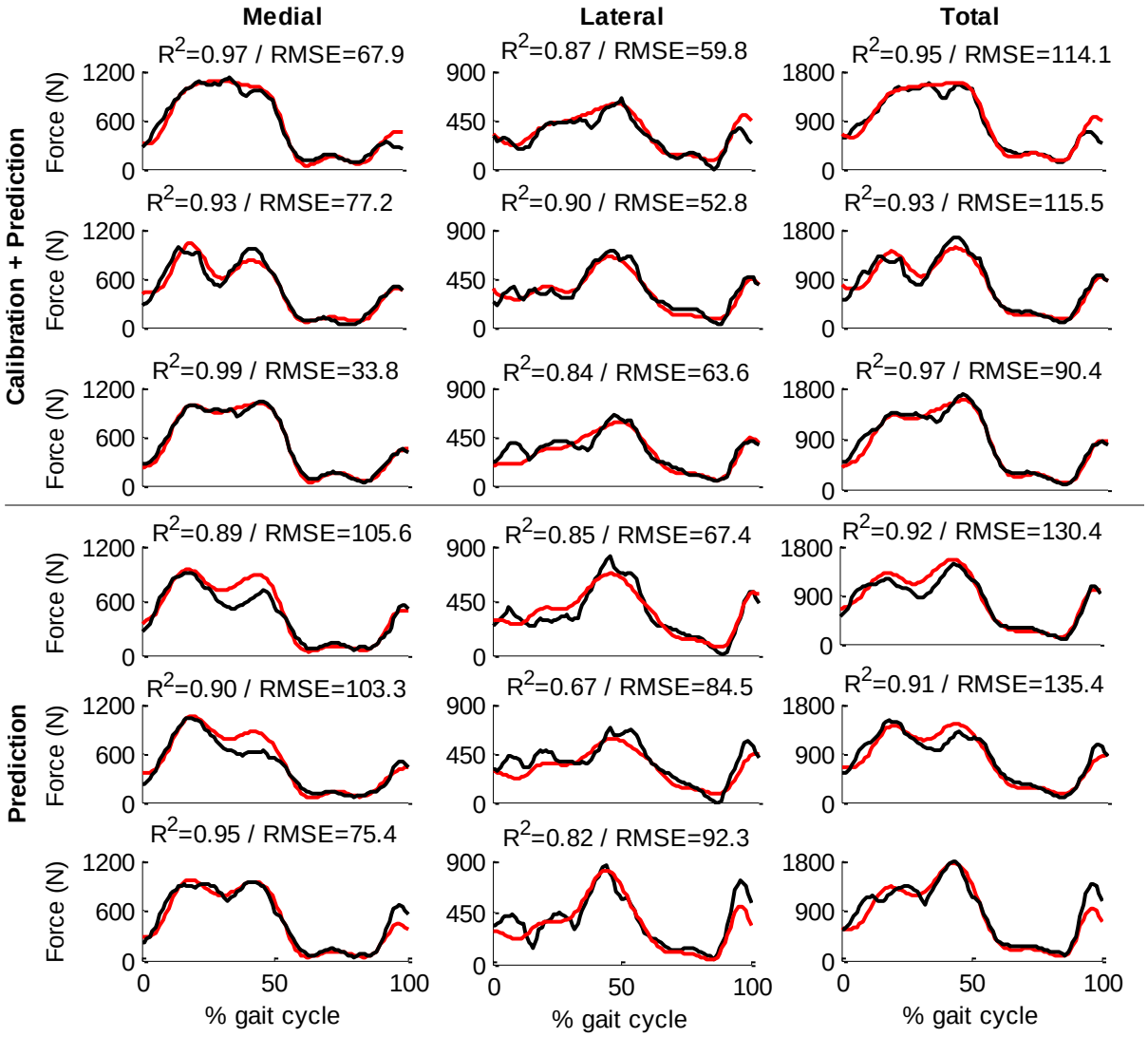

Figure A.1. Knee contact force predictions (Medial, Lateral and Total) for the three gait trials where these forces were used during the calibration (Calibration + Prediction) and for other three gait trials using the same set of muscle parameters (Prediction).

Appendix B: Publications

Publications derived from the PhD thesis

Journal articles

Serrancolí G., Kinney A.L., Fregly B.J., Font-Llagunes J.M. Two-step optimization problem formulation for predicting knee muscle and contact forces during gait. To be submitted to the *Journal of Biomechanics*.

Serrancolí G., Monllau J.C., Font-Llagunes J.M. Analysis of the Activation-Deactivation Pattern and Muscle Synergies in ACL-Deficient Subjects during Gait. Submitted to the journal of *Clinical Biomechanics*.

Serrancolí G., Font-Llagunes J.M., Barjau A. A weighted cost function to deal with the muscle force sharing problem in injured subjects: A single case study. *Proceedings of the Institution of Mechanical Engineers, Part K: Journal of Multi-body Dynamics* 2014, 228:241–251.

Congress presentations

Serrancolí G., Kinney A.L., Fregly B.J., Font-Llagunes J.M. How do in vivo knee contact force data affect calibration of muscle-tendon model parameter values? *VI International Conference on Computational Bioengineering*. Barcelona (Catalonia), September 2015. Submitted.

Serrancolí G., Kinney A.L., Fregly B.J., Font-Llagunes J.M. What can knee contact force data teach us about calibration of muscle-tendon model parameter values? *Summer Biomechanics, Bioengineering and Biotransport Conference*. Snowbord, Utah (USA), June 2015. Submitted.

Serrancolí G., Kinney A.L., Fregly B.J., Font-Llagunes J.M. Sinergy-based two-level optimization for predicting knee contact forces during walking. *25th Congress of the International Society of Biomechanics*. Edinburg (UK), July 2015. Accepted.

Serrancolí G., Monllau J.C., Font-Llagunes J.M. A comparative study of the muscle synergy patterns in healthy and ACL-deficient subjects. *25th Congress of the International Society of Biomechanics*. Edinburg (UK), July 2015. Accepted.

Serrancolí G., Kinney A.L., Fregly B.J., Font-Llagunes J.M. Prediction of knee contact forces using synergy-based two-level optimization. *ECCOMAS Thematic Conference on Multibody Dynamics*. Barcelona (Catalonia), June 2015. Accepted.

Serrancolí, G. Analysis of the Force–Sharing Problem in the Biomechanics of Human Motion. *2a Jornada d'Investigadors Predoctorals Interdisciplinària.* Barcelona, February 2014.

Serrancolí, G., Walter, J.P., Kinney, A.L., Barjau, A., Fregly, B.J., Font-Llagunes, J.M. Formulation to predict lower limb muscle forces during gait. *III Reunión del Capítulo Español de la Sociedad Europea de Biomecánica (ESB).* Barcelona (Catalonia), October 2013.

Serrancolí, G., Walter, J.P., Kinney, A.L., Fregly, B.J., Font-Llagunes, J.M. Optimization problem formulation for predicting knee muscle and contact forces during gait. *XIV International Symposium on Computer Simulation in Biomechanics.* Natal (Brazil), August 2013.

Serrancolí, G., Font-Llagunes, J.M., Barjau, A. Determination of the strategy for solving the muscle force sharing problem in patients suffering ACL rupture. *Congress on Numerical Methods in Engineering.* Bilbao (Spain), June 2013.

Serrancolí, G., Font-Llagunes, J.M., Barjau, A. On the force sharing problem in patients suffering joint pain. *18th Congress of the European Society of Biomechanics.* Lisbon (Portugal), July 2012.

Other congress presentations in line with the research of the thesis

Tassani S., Peiret A., Bosch E., Serrancolí S., Font-Llagunes J.M., Noailly J. A multi-scale study of the hip joint mechanics: influence of inertial forces. 21st Congress of the European Society of Biomechanics. Prague (Czech Republic), July 2015. Submitted.

Ilzarbe A., Serrancolí G., Font-Llagunes J.M. Simulation of active orthosis-assisted gait considering user-device cooperation and interface contact forces. *ECCOMAS Thematic Conference on Multibody Dynamics*. Barcelona (Catalonia), June 2015. Accepted.

Ilzarbe A., Serrancolí G., Font-Llagunes J.M. A dynamic analysis of an integrated lower limb-orthosis biomechanical model for interface contact pressures estimation. *IV Reunión del Capítulo Español de la Sociedad Europea de Biomecánica (ESB).* Valencia (Spain), November 2014.

Peiret, A., Bosch, E., Serrancolí, G., Noailly, J., Font-Llagunes, J.M. Multiscale analysis of the hip joint: translate mechanical information from inverse analyses of body motion into boundary loads for finite element calculations of organ/tissue biomechanics. *7th Annual Symposium on Bioengineering and Nanomedicine.* Barcelona (Catalonia), September 2014.

Peiret, A., Bosch, E., Serrancolí, G., Noailly, J., Font-Llagunes, J.M. A multi-scale study of the hip joint mechanics using rigid-body inverse dynamics and finite element analysis. *WCCM XI - ECCM V - ECFD VI Congress*. Barcelona (Catalonia), July 2014.

Font-Llagunes, J.M., Arroyo, G., Serrancolí, G., Romero, F. A powered lower limb orthosis for gait assistance in incomplete spinal cord injured subjects. *4th International Symposium on Applied Sciences in Biomedical and Communication Technologies.* Barcelona (Catalonia), October 2011.

References

[1] Serrancolí G, Font-Llagunes JM, Barjau A. A weighted cost function to deal with the muscle force sharing problem in injured subjects: A single case study. *Proceedings of the Institution of Mechanical Engineers, Part K: Journal of Multi-body Dynamics* 2014, 228:241–251.

[2] Besier TF, Fredericson M, Gold GE, Beaupré GS, Delp SL. Knee muscle forces during walking and running in patellofemoral pain patients and pain-free controls. *Jorunal of Bimechanics* 2009; 42:898-905.

[3] Dhaher YY, Kahn LE. The Effect of Vastus Medialis Forces on Patello-femoral Contact: A Model-based Study. *Journal of Biomechanical Engineering* 2002; 124**:**758-767.

[4] Font-Llagunes JM, Pàmies-Vilà R, Alonso J, Lugrís U. Simulation and design of an active orthosis for an incomplete spinal cord injured subject. *Procedia IUTAM* 2011; 2:68-81.

[5] Van den Bogert AJ. Exotendons for assistance of human locomotion. *Biomedical Engineering Online* 2003; 2:17.

[6] Ackermann M. Dynamics and energetics of walking with prostheses. *PhD thesis. University of Stuttgart, Germany*, 2008.

[7] De Vita P, Hortobagyi T. Functional knee brace alters predicted knee muscle and joint forces in people with ACL reconstruction during walking. *Journal of Applied Biomechanics* 2001, 17:297–311.

[8] Hardt DE. Determining muscle forces in the leg during normal human walking—an application and evaluation of optimization methods. *Journal of Biomechanical Engineering* 1978; 100:72–78.

[9] Erdemir A, McLean S, Herzog W, Van den Bogert AJ. Model-based estimation of muscle forces exerted during movements. *Clinical Biomechanics* 2007, 22:131–154.

[10] Crowninshield RD, Brand RA. A physiologically based criterion of muscle force prediction in locomotion. *Journal of Biomechanics* 1981; 14:793–801.

[11] Heintz S, Gutierrez-Farewik EM. Static optimization of muscle forces during gait in comparison to EMG-to-force processing approach. *Gait & posture* 2007; 26:279–288.

[12] Zajac FE. Muscle and tendon: properties, models, scaling, and application to biomechanics and motor control. *Critical reviews in biomedical engineering* 1989, 17: 359–411.

[13] Hill A. 1938. The heat of shortening and the dynamic constants of muscle. *Proceedings of the Royal Society of London. Series B, Biological Sciences* 1938, 126: 136–195.

[14] Konrad P. *The ABC of EMG. A Practical Introduction to Kinesiological Electromyography*. 1st ed. Scottsdale: Noraxon, 2005, p.60.

[15] Riemann B, Lephart S. The sensorimotor system, part II: the role of proprioception in motor control and functional joint stability. *Journal of Athletic Training* 2002; 37**:**80–84.

[16] Delp SL, Anderson FC, Arnold AS, Loan P, Habib A, John CT, Guendelman E, Thelen DG. OpenSim: open-source software to create and analyze dynamic simulations of movement. *IEEE transactions on bio-medical engineering* 2007; 54**:**1940–50.

[17] Delp SL, Loan JP, Hoy MG, Zajac FE, Topp EL, Rosen JM. An interactive graphics-based model of the lower extremity to study orthopaedic surgical procedures. *IEEE transactions on bio-medical engineering* 1990; 37:757–767.

[18] Menegaldo LL, Fleury AT, Weber HI. Biomechanical modeling and optimal control of human posture. *Journal of biomechanics* 2003; 36:1701–1712.

[19] Van Soest AJ, Bobbert MF. The contribution of muscle properties in the control of explosive movements. *Biological Cybernetics* 1993; 69**:**195–204.

[20] Glitsch U, Baumann W. The three-dimensional determination of internal loads in the lower extremity. *Journal of Biomechanics* 1997; 30:1123–1131.

[21] Lugrís U, Carlín J. Solution methods for the double-support indeterminacy in human gait. *Multibody System Dynamics* 2013; 30:247-263.

[22] Cerveri P, Lopomo N, Pedotti A. Derivation of centers and axes of rotation for wrist and fingers in a hand kinematic model: Methods and reliability results. *Annals of Biomedical Engineering* 2005; 33:402–412.

[23] Hansen N, Müller SD, Koumoutsakos P. Reducing the time complexity of the derandomized evolution strategy with covariance matrix adaptation (CMA-ES). *Evolutionary Computation* 2003, 11:1–18.

[24] Hermens H, Freriks B. Development of recommendations for SEMG sensors and sensor placement procedures. *Journal of Electromyography and Kinesiology* 2000; 10:361–74.

[25] Merletti, R. Standards for reporting EMG data. *Journal of Electromyography and Kinesiology* 1999; 9:1.

[26] Rudolph KS, Eastlack ME, Axe MJ, Snyder-Mackler L. Movement patterns after anterior cruciate ligament injury: a comparison of patients who compensate well for the injury and those who require operative stabilization. *Journal of Electromyography and Kinesiology* 1998; 8:349–362.

[27] Chmielewski TL, Hurd WJ, Rudolph KS, Axe MJ, Snyder-Mackler L. Perturbation training improves knee kinematics and reduces muscle cocontraction after complete unilateral anterior cruciate ligament rupture. *Physical Therapy* 2005; 85:740-749.

[28] Winter DA. *Biomechanics and Motor Control of Human Movement*. 3rd ed. Waterloo: University of Waterloo, 2005; p.143.

[29] Hurd WJ, Snyder-Mackler L. Knee instability after acute ACL rupture affects movement patterns during the mid-stance phase of gait. *Journal of Orthopedic Research* 2007; 25:1369–1377.

[30] Berchuck M, Andriacchi TP, Bach BR, Reider B. Gait adaptations by patients who have a deficient anterior cruciate ligament. *J. Bone Joint Surg. Am.* 1990; 72:871–877.

[31] Beard DJ, Soundarapandian RS, O'Connor JJ, Dodd CAF. Gait and electromyographic analysis of anterior cruciate ligament deficient subjects. *Gait & Posture* 1996; 4:83–88.

[32] Gardinier ES, Manal K, Buchanan TS, Snyder-Mackler L. Gait and neuromuscular asymmetries after acute anterior cruciate ligament rupture. *Medicine & Sience in Sports & Exercise* 2012; 44:1490-1496.

[33] Botasso CL, Prilutsky BI, Croce A, Imberti E, Sartirana S. A numerical procedure for inferring from experimental data the optimization cost functions using a multibody model of the neuro-musculoskeletal system. *Multibody System Dynamics* 2006; 16:123-154.

[34] Ting LH. Dimensional reduction in sensorimotor systems: a framework for understanding muscle coordination of posture. *Progress in brain research* 2007; 165:299–321.

[35] Ting LH, McKay JL. Neuromechanics of muscle synergies for posture and movement. *Current opinion in neurobiology* 2007; 17:622–628.

[36] Ting LH, Chvatal SA, Safavynia SA, Mckay JL. Review and perspective : neuromechanical considerations for predicting muscle activation patterns for movement. *International Journal for numerical methods in biomedical engineering* 2012; 28:1003-1014.

[37] Lacquaniti F, Ivanenko YP, Zago M. Patterned control of human locomotion. *The Journal of physiology* 2012; 590:2189–2199.

[38] Ting LH, Macpherson JM. A limited set of muscle synergies for force control during a postural task. *Journal of neurophysiology* 2005; 93:609–613.

[39] Lee DD, Seung HS. Learning the parts of objects by non-negative matrix factorization. *Nature* 2000; 401:788–791.

[40] Clark D, Ting LH, Zajac FE, Neptune RR, Kautz SA. Merging of healthy motor modules predicts reduced locomotor performance and muscle coordination complexity post-stroke. *Journal of neurophisiology* 2010; 103:844-857.

[41] Ivanenko YP, Poppele RE, Lacquaniti F. Five basic muscle activation patterns account for muscle activity during human locomotion. *The Journal of physiology* 2004; 556:267–282.

[42] De Groote F, Jonkers I, Duysens J. Task constraints and minimization of muscle effort result in a small number of muscle synergies during gait. *Frontiers in Computational Neuroscience* 2014; 8**:**1–11.

[43] Allen JL, Neptune RR. Three-dimensional modular control of human walking. *Journal of biomechanics* 2012; 45:2157–2163.

[44] Ivanenko YP, Cappellini G, Dominici N, Poppele RE, Lacquaniti F. Coordination of locomotion with voluntary movements in humans. *The Journal of neuroscience* 2005; 25:7238–7253.

[45] Oliveira AS, Gizzi L, Farina D, Kersting UG. Motor modules of human locomotion: influence of EMG averaging, concatenation, and number of step cycles. *Frontiers in human neuroscience* 2014; 8:335.

[46] Neptune R, Clark D, Kautz S. Modular control of human walking: a simulation study. *Journal of biomechanics* 2009; 42:1282–1287.

[47] Dominici N, Ivanenko YP, Cappellini G, D'Avella A, Mondì V, Cicchese M, Fabiano A, Silei T, Di Paolo A, Giannini C, Poppele R E, Lacquaniti F. Locomotor primitives in newborn babies and their development. *Science* 2011; 334:997–999.

[48] De Rugy A, Loeb GE, Carroll TJ. Are muscle synergies useful for neural control?. *Frontiers in computational neuroscience* 2013; 7**:**19.

[49] Erdemir A, McLean S, Herzog W, Van den Bogert AJ. Model-based estimation of muscle forces exerted during movements. *Clinical Biomechanics* 2007; 22:131–154.

[50] Walter JP, Kinney AL, Banks SA, D'Lima DD, Besier TF, Lloyd DG, Fregly BJ. Muscle synergies may improve optimization prediction of knee contact forces during walking. *Journal of Biomechanical Engineering* 2014; 136:021031.

[51] Rudolph KS, Axe MJ, Buchanan TS, Scholz JP, Snyder-Mackler L. Dynamic stability in the anterior cruciate ligament deficient knee. *Knee Surgery, Sports Traumatology, Arthroscopy* 2001; 9:62–71.

[52] Knoll Z, Kiss RM, Kocsis L. Gait adaptation in ACL deficient patients before and after anterior cruciate ligament reconstruction surgery. *Journal of Electromyography and Kinesiology* 2004; 14:287–294.

[53] Houck JR, Wilding GE, Gupta R, De Haven KE, Maloney M. Analysis of EMG patterns of control subjects and subjects with ACL deficiency during an unanticipated walking cut task. *Gait & posture* 2007; 25:628–638.

[54] Button K, Van Deursen R, Price P. Classification of functional recovery of anterior cruciate ligament copers, non-copers, and adapters. *British Journal of sports medicine* 2006; 40:853–858.

[55] Kendall FP, McCreary EK, Provance PG, Rodgers MM, Romani WA. Muscles, testing and function: with posture and pain. 5th ed. Philadelphia: Lippincott Williams & Wilkins, 2005.

[56] Courtney C, Rine R, Kroll PG. Central somatosensory changes and altered muscle synergies in subjects with anterior cruciate ligament deficiency. *Gait & posture* 2005; 22:69–74.

[57] Chmielewski TL, Rudolph KS, Fitzgerald GK, Axe MJ, Snyder-Mackler L. Biomechanical evidence supporting a differential response to acute ACL injury. *Clinical Biomechanics* 2001; 16:586–591.

[58] Ferber R, Osternig L, Woollacott MH, Wasielewski NJ, Lee JH. Gait mechanics in chronic ACL deficiency and subsequent repair. *Clinical Biomechanics* 2002; 17:274–285.

[59] World Health Report. 2015. *National Health Organization*. [ONLINE] Available at: http://www.who.int/en/. [Accessed 12 February 15].

[60] Vos T, Flaxman AD, Naghavi M, Lozano R, Michaud C, Ezzati M, Shibuya K, Salomon J, Abdalla S, Aboyans V et al. Years lived with disability (YLDs) for 1160 sequelae of 289 diseases and injuries 1990-2010: a systematic analysis for the Global Burden of Disease Study 2010. *Lancet* 2012; 380**:**2163–2196.

[61] Verghese J, LeValley A. Epidemiology of gait disorders in community-residing older adults. *Journal of the American Geriatics Society* 2006; 54:255–261.

[62] States RA, Pappas E, Salem Y. Overground Physical Therapy Gait Training for Chronic Stroke Patients With Mobility Deficits," Cochrane Database Syst Rev 2009, 40:627–628.

[63] Buckwalter J, Stanish W. The increasing need for nonoperative treatment of patients with osteoarthritis. *Clinical Orthopaedics & Related Research* 2001; 385: 36-45.

[64] Mizner RL, Snyder-Mackler L. Altered loading during walking and sit-to-stand is affected by quadriceps weakness after total knee arthroplasty. *Journal of Orthopaedic Reserach* 2005; 23:1083–1090.

[65] Fregly BJ, Reinbolt JA, Rooney KL, Mitchell KH, Chmielewski TL. Design of patient-specific gait modifications for knee osteoarthritis rehabilitation. *IEEE transactions on bio-medical engineering* 2007; 54:1687–1695.

[66] Gerus P, Sartori M, Besier TF, Fregly BJ, Delp SL, Banks SA, Pandy M. G. D'Lima DD, Lloyd DG. Subject-specific knee joint geometry improves predictions of medial tibiofemoral contact forces. *Journal of biomechanics* 2013; 46:2778–2786.

[67] Wesseling M, Derikx L, De Groote F, Bartels W, Meyer C, Verdonschot N, Jonkers I. Muscle optimization techniques impact the magnitude of calculated hip joint contact forces. *Journal of Orthopaedic Reserach* 2014; doi:10.1002/jor.22769.

[68] Arnold E, Ward S, Lieber R, and Delp S. A model of the lower limb for analysis of human movement. *Annals of biomedical engineering* 2010; 38:269–279.

[69] Horsman MDK, Koopman HFJM., Van der Helm FCT, Prosé LP, Veeger HEJ. Morphological muscle and joint parameters for musculoskeletal modelling of the lower extremity. *Clinical biomechanics* 2007; 22:239–247.

[70] Lloyd DG, Besier TF. An EMG-driven musculoskeletal model to estimate muscle forces and knee joint moments in vivo," *Journal of Biomechanics* 2003; 36:765–776.

[71] Shao Q, Bassett D, Manal K, Buchanan T. An EMG-driven model to estimate muscle forces and joint moments in stroke patients. *Computers in biology and medicine* 2009; 39:1083–1088.

[72] Sartori M, Reggiani M, Farina D, Lloyd DG. EMG-driven forward-dynamic estimation of muscle force and joint moment about multiple degrees of freedom in the human lower extremity. *PloS one* 2012; **7**:e52618.

[73] Routson RL, Kautz SA, Neptune RR. Modular organization across changing task demands in healthy and poststroke gait. *Physiological reports* 2014; 2:1–14.

[74] Ivanenko YP, Cappellini G, Dominici N, Poppele RE, Lacquaniti F. Coordination of locomotion with voluntary movements in humans. *The Journal of Neuroscience* 2005; 25:7238–7253.

[75] Rodriguez KL, Roemmich RT, Cam B, Fregly BJ, Hass CJ. Persons with Parkinson's disease exhibit decreased neuromuscular complexity during gait. *Clinical neurophysiology* 2013; 124:1390–1397.

[76] Bianco, NA, Kinney AL, Fregly BJ. Predicting unmeasured muscle excitations from measured muscle synergies. *Proceedings of the 7th World Congress of Biomechanics* 2014, Boston, MA.

[77] Fregly BJ, Besier T, Lloyd D. Grand challenge competition to predict in vivo knee loads. *Journal of Orthopaedic Research* 2012; 30:503–513.

[78] Bergmann G, Bender A, Graichen F, Dymke J, Rohlmann A, Trepczynski A, Heller MO, Kutzner I. Standardized loads acting in knee implants. *PloS one* 2014; 9: e86035.

[79] D'Lima DD, Townsend CP, Arms SW, Morris BA, Colwell CW. An implantable telemetry device to measure intra-articular tibial forces. *Journal of Biomechanics* 2005; 38:299–304.

[80] Kristianslund E, Krosshaug T, Van den Bogert AJ. Effect of low pass filtering on joint moments from inverse dynamics: implications for injury prevention. *Journal of biomechanics* 2012; 45:666–671.

[81] He J, Levine WS, Loeb GE. Feedback gains for correcting small perturbations to standing posture. *IEEE Transactions on Automatic Control* 1991; 36:322–332.

[82] Winters J, Stark L. Estimated mechanical properties of synergistic muscles involved in movements of a variety of human joints. *Journal of biomechanics* 1988; 21:1027–1041.

[83] Ting L, Chvatal S. Decomposing muscle activity in motor tasks: methods and interpretation. "*Motor Control: Theories, Experiments and Applications*". 1st ed. New York: Oxford University Press, 2010; p. 37.

[84] Delp SL, Anderson FC, Arnold AS, Loan P, Habib A, John CT, Guendelman E, Thelen DG. OpenSim: open-source software to create and analyze dynamic simulations of movement. *IEEE transactions on bio-medical engineering* 2007; 54:1940–1950.

[85] Bei Y, Fregly BJ. Multibody dynamic simulation of knee contact mechanics. *Medical engineering & physics* 2004; 26:777–789.

[86] Arnold EM, Hamner SR, Seth A, Millard M, Delp SL. How muscle fiber lengths and velocities affect muscle force generation as humans walk and run at different speeds. *The Journal of experimental biology* 2013; 216:2150–2160.

[87] Kaufman K, An K, Litchy W, and Chao E. Physiological prediction of muscle forces—I. Theoretical formulation. *Neuroscience* 1991; 40:781:792.

[88] Arnold E, Delp S. Fibre operating lengths of human lower limb muscles during walking. *Philosophical Transactions of the Royal Society* B 2011; 366:1530–1539.

[89] Rubenson J, Pires NJ, Loi HO, Pinniger GJ, Shannon DG. On the ascent: the soleus operating length is conserved to the ascending limb of the force-length curve across gait mechanics in humans. *The Journal of experimental biology* 2012; 215:3539–3551.

[90] Kinney A. Update on grand challenge competition to predict in vivo knee loads. *Journal of Biomechanical Engineering* 2013; 135:021012.

[91] Manal K, Buschanan TS. An electromyogram-driven musculoskeletal model of the knee to predict *in vivo* joint contact forces during normal and novel gait patterns. *Journal of Biomechanical Engineering* 2013; 135:021014.

[92] Shelburne KB, Torry MR, Pandy MG. Muscle, Ligament, and joint-contact forces at the knee during walking. *Medicine & Science in Sports & Exercise* 2005; 37:1948–1956.